

**DEVELOPMENT OF A
CONTACT FATIGUE MODEL FOR
CONTINUOUSLY VARIABLE TRANSMISSIONS**

18-month project for
TOROTRAK DEVELOPMENT LTD

Final Report

by

George K. Nikas

Imperial College of Science, Technology and Medicine
Mechanical Engineering Department, Tribology section
Exhibition Road, London, SW7 2BX

December 1999

ACKNOWLEDGEMENTS

The author wishes to thank Dr Richard Sayles of Imperial College (Mechanical Engineering Department, Tribology section) for organising this project and dealing with all the technicalities and bureaucratic formalities. Dr Sayles acted as the academic supervisor in this project and hosted the meetings between the author and the representative of TOROTRAK throughout the period of the work.

The author also wishes to thank Mr Mervyn Patterson of TOROTRAK DEVELOPMENT LTD, who was the industrial supervisor in this project, for his collaboration and for his prompt replies to all queries and requests of experimental data and other information on the design and operation of TOROTRAK's IVT.

CONTENTS

LIST OF SYMBOLS	4
1. Introduction	7
2. Parameters of the CVT model	9
2.1 Lubricant thermal effects	10
2.2 Thermal stresses from asperity interactions	11
2.3 Lubricant non-Newtonian effects	12
2.4 Surface roughness effects	13
2.5 Transient effects	14
3. Solution of the lubrication problem	15
3.1 Development of a generalised lubrication equation	15
3.2 Lubricant rheology models	21
3.2.1 Newtonian rheology model and lubricant viscosity	21
3.2.2 Bair and Winer (1979) rheology model	23
3.2.3 Gecim and Winer (1980) rheology model	24
3.2.4 Elsharkawy and Hamrock (1991) rheology model	25
3.3 Lubricant limiting shear stress	26
3.4 Lubricant shear stress components	27
3.5 Lubricant density	28
3.6 Geometry of the contact	29
3.7 Film thickness (geometry, roughness and elastic deformations)	31
3.8 Boundary and other conditions	37
4. Stress analysis	38
5. Fatigue life equation	42
5.1 Deformation Energy (von Mises) fatigue stress criterion	43
5.2 Maximum Shear Stress criterion	44
6. Contact fatigue – comparison of rolling bearings and CVTs	46
7. Examples	49
7.1 An example with extensive asperity interactions	57
7.2 An example of the subsurface stress fields	61
8. Discussion and suggestions	66
9. Computer program (“TORO.EXE”, version 1.0.0 beta)	70
REFERENCES	76

LIST OF SYMBOLS

A	Proportionality constant (see equation (5.1)).
A_1, A_2	Integration variables (equations (3.6)).
c	Stress criterion exponent (see equation (5.1)).
$c_{z,x}, c_{z,y}$	Auxiliary variables (equations 3.9)).
$c_{zz,x}, c_{zz,y}$	Auxiliary variables (equations 3.9)).
c_1, c_2, c_3	Constants of the lubricant density formula (see equation (3.36)).
C_1, C_2, C_3	Auxiliary variables (equations (5.7)-(5.8)).
d	Auxiliary variable (see equations (3.19)).
$d_{z,x}, d_{z,y}$	Auxiliary variables (see equations (3.19)).
$d_{zz,x}, d_{zz,y}$	Auxiliary variables (see equations (3.19)).
D	Distance between two cooperating surfaces (equation (3.46)).
D_e	Combined normal elastic displacements of the cooperating surfaces.
D_p	Combined normal plastic displacements of the cooperating surfaces.
D_x, D_y	Lengths of the contact ellipse semi-axes x and y.
e	Variable defined in equation (3.39).
e'	Life exponent (Weibull slope).
E	Effective modulus of elasticity (equation (3.42)).
$E_{\text{roller}}, E_{\text{disk}}$	Moduli of elasticity of the roller and the toroidal disk.
$E(e)$	Complete elliptic integral of the second kind of argument e (equations (3.40)).
F_1	Auxiliary variable (equation (4.10)).
G	Shear modulus of elasticity.
G_1	Auxiliary variable (equation (4.11)).
h	Film thickness (see figure 3.1).
h'	Depth exponent (see equation (5.1)).
h_{min}	Minimum lubricant film thickness.
H	“Height” of the variator (see figure 7.3).
H_1	Auxiliary variable (equation (4.12)).
J_1, J_2, J_3	Stress invariants (equations (5.6)).
$K(e)$	Complete elliptic integral of the first kind of argument e (equations (3.40)).

N	Number (millions) of stress cycles (equation (5.3)).
p	Pressure.
p_0	Maximum Hertzian pressure.
p_H	Hydrostatic pressure ($p_H = J_1/3$).
P	Load (supported, transmitted).
P_s	Load supported by solid contact.
r	“Radius” of the variator (see figure 7.3).
$r_x^{(\text{disk})}, r_y^{(\text{disk})}$	Radii of curvature of the toroidal disk’s working surface in directions x and y.
$r_x^{(\text{roller})}, r_y^{(\text{roller})}$	Radii of curvature of roller’s working surface in directions x and y.
R_{max}	Maximum peak-to-valley height of surface roughness.
R_x, R_y	Effective radii of curvature (equations (3.37)).
s	Lubricant internal shear strain rate.
S	Probability of survival ($0 < S < 1$; equation (5.4)).
S_0	Lubricant (Roelands) viscosity-temperature coefficient (see equation (3.24)).
t	Time.
u	Fluid speed in direction x (see figure 3.1).
\bar{u}_z	Normal elastic surface displacement.
v	Fluid speed in direction y (see figure 3.1).
V_R	Risk volume (volume where $ \sigma > \sigma_u$) (see equation (5.1)).
w	Fluid speed in direction z (see figure 3.1).
Y	Yield stress in simple tension.
z'	Stress-weighted average depth (see equation (5.1)).
Z_1	Lubricant (Roelands) viscosity-pressure coefficient (see equation (3.24)).
α	Lubricant (Barus) pressure-viscosity coefficient.
γ	Constant of the limiting shear stress function (see equation (3.35)).
δ	Constant of the limiting shear stress function (see equation (3.35)).
ζ	Combined surface roughness (equation 3.47)).
$\zeta_{\text{roller}}, \zeta_{\text{disk}}$	Roughness of the roller and the toroidal disk.

η	Fluid dynamic viscosity.
η_x, η_y	Fluid equivalent dynamic viscosity in directions x and y.
η_0	Absolute viscosity at $p = 0$ and at ambient temperature.
ϑ	Angle.
θ	Lubricant temperature.
θ_0	Environmental temperature.
λ	Lambda ratio, the ratio of the minimum film thickness to the composite RMS surface roughness.
Λ	Parameter of the Elsharkawy-Hamrock rheology model (see equation (3.32)).
μ	Boundary-lubrication friction coefficient.
μ_{disk}	Calculated traction coefficient for the toroidal disk.
μ_{roller}	Calculated traction coefficient for the roller.
$\nu_{\text{roller}}, \nu_{\text{disk}}$	Poisson ratios of the roller and the toroidal disk.
ρ	Fluid density.
ρ_0	Fluid density at ambient conditions (zero pressure and environmental temperature).
$\sigma_1, \sigma_2, \sigma_3$	Principal normal stresses (equations (5.9)).
σ_u	Endurance stress limit (see equation (5.1)).
τ	Shear stress.
τ_0	Constant of the limiting shear stress function (see equation (3.35)).
τ_L	Lubricant limiting shear stress.
τ_{max}	Maximum shear stress.
$\bar{\tau}_{zx}, \bar{\tau}_{zy}$	Surface tractions in directions x and y.
φ	Working angle (see figure 7.3).
Ω	Auxiliary variable (equation (4.13)).

1. Introduction

A contact fatigue model for rolling bearings was established as early as in the 1940s by Lundberg and Palmgren, who successfully predicted the life expectancy of rolling bearings of their era. That model has been extensively used by other bearing manufactures and became an ISO standard, still being in use, with some life adjustment factors to account for the improved quality of modern steels and methods of manufacture. Ioannides and Harris (1985) extended the original Lundberg-Palmgren model and their model has been widely adopted not only for rolling bearings but for other Machine Elements as well (gears, CVTs etc).

In the case of TOROTRAK, there was the need to develop a contact fatigue model to study the operation of its patented Infinitely Variable Transmission (IVT) and, specifically, the life expectancy of the main components of the variator of the IVT system (shown in figure 1.1), namely the rollers and the toroidal disks.

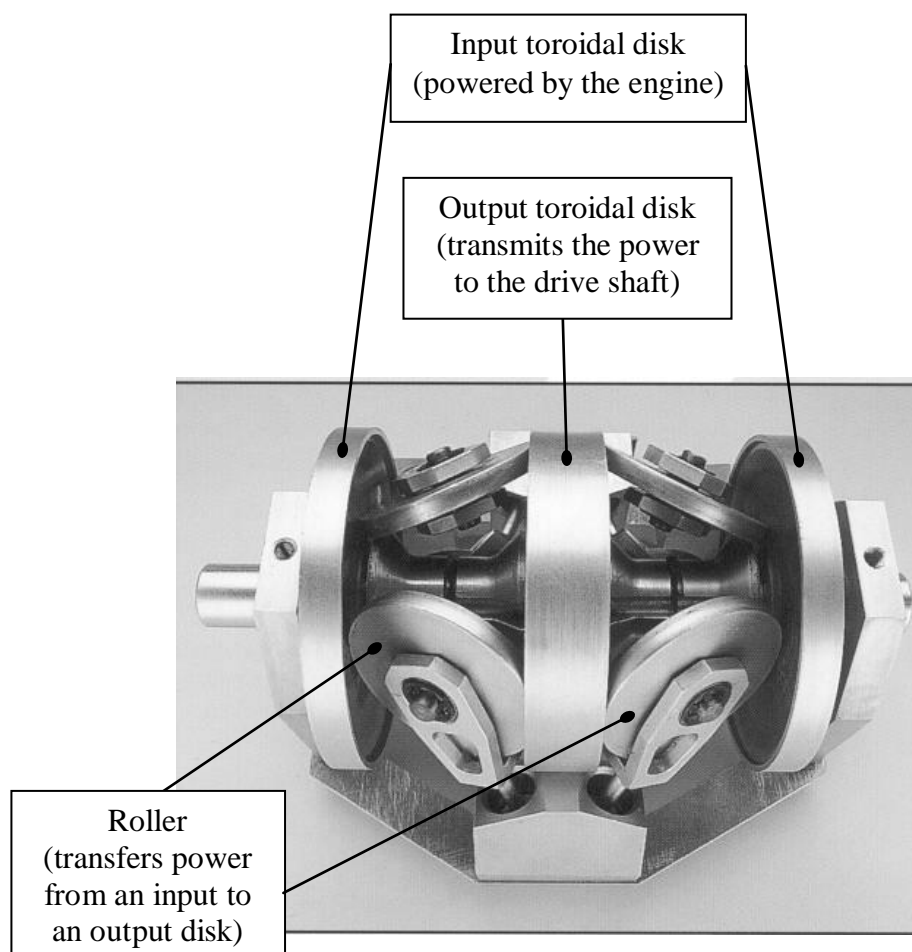


Figure 1.1 The TOROTRAK variator.

The variator is the heart of the transmission and its operation is crucial for the whole system. TOROTRAK has developed a test rig to simulate the operation of the variator and was in need of a theoretical model to predict analytically the lubrication and loading conditions that determine the fatigue lives of the rollers and the toroidal (input and output) disks. After discussions between Dr Richard Sayles of Imperial College and Mr Mervyn Patterson of TOROTRAK, it was agreed that such a theoretical model *could* be developed, based on the theoretical background and expertise in the Tribology Section of the Mechanical Engineering Department of Imperial College. It was agreed that the model should be in the form of computer software that can evaluate the lubrication, mechanical loading (stress analysis) and fatigue lives of the vital components of the variator (rollers and disks), based on input such as the basic geometrical parameters, real surface roughness, sliding speeds, material properties, transmitted load, etc. Furthermore, the software would be used to draw conclusions regarding the importance of the various parameters of the model (for example the importance of the lambda ratio) and, thus, provide guidelines in the development of a CVT rig.

The author was appointed as the researcher of this 18-month project and undertook the task of developing the theoretical model and the accompanying computer code. The computer code is specifically written for CVTs and remains intellectual (Copyright) property of the author, with full permission for its use given only to TOROTRAK DEVELOPMENT LTD.

In the next pages, a complete description of the model is presented together with examples/applications of the computer program, followed by suggestions for future work and an extensive list of references.

2. Parameters of the CVT model

The lubrication of CVTs is the most theoretically challenging task among all similar problems in Machine Elements (bearings, gears etc). This is because of the following reasons.

- (1) The contact geometry is two dimensional (elliptical contact).
- (2) The contact operates under mixed rolling-sliding/spinning conditions.
- (3) The surfaces are rough, rougher than in bearings but usually not as rough as in gears.
- (4) The fluid pressures are normally high (usually higher than 1 GPa).
- (5) Because of the sliding/spinning and high shear strain rates in the lubricant, non-Newtonian characteristics of the lubricant must be accounted for.
- (6) Because of the traction nature of CVTs, there are fluid thermal effects that can not be ignored.
- (7) The contacts often operate in the partial or even boundary lubrication regime (film thickness less than 0.5-1 μm , lambda ratio less than 3-5).
- (8) There are often roughness asperity interactions, which give rise to local frictional heating and complicated thermoelastic/plastic events at asperity scales.
- (9) There are transient effects that must be taken into account (rapid changes of the transmitted load, speeds and contact geometry).

The above characteristics infer that the only lubrication equation which can effectively describe such problems is the Reynolds equation *in its most general form*, without any simplifications. The Reynolds equation is a partial differential equation, which has the great disadvantage of being very unstable during numerical manipulation, requiring significant amounts of computing power and memory to overcome its instability with the use of dense grids, especially when dealing with rough surfaces and transient processes. The numerical solution of the Reynolds equation has been in the frontier of Tribology for the last 30 years and, even at the end of the 20th century, there are still many unanswered questions regarding the explanation of the numerical results obtained with different methods. At the time of writing this report (November 1999), no one has yet come forward to present a numerical solution of the general equation, although there are a few research teams world-wide that are very close to this landmark.

In the frame of the current 18-month project, and based on the author's prior experience on this field, it was decided that the available time was barely sufficient to develop a numerical method to solve the general Reynolds equation, with fluid and asperity thermal effects being left out of the model. Both of the previous two effects are expected to have a role in the life expectancy of a CVT. Below, a brief discussion of the various aspects affecting the lubrication of a CVT is presented together with the reasoning behind the selection of which aspects are incorporated in and which are excluded from the present model.

2.1 Lubricant thermal effects

In a sliding/spinning contact like the contact of a CVT, the lubricant is sheared internally and, hence, heated. There is also a very small amount of heat produced due to the compression of the lubricant when passing through the high pressure (central) zone of the contact. The internal friction coefficient of the lubricant depends on the nature of the lubricant itself, but a value of around 0.06 for mineral oils is generally agreeable. Because of the high lubricant pressures experienced in heavily loaded CVT contacts (pressures over 1 GPa), even a small friction coefficient of 0.06 accounts for lubricant heating that results in local (internal) lubricant flash temperatures (temperature increments over the bulk temperature) of 50-100 °C. If the bulk temperature is taken into account (for a CVT this could roughly be between 50-100 °C), the overall local lubricant temperature could be as high as 200 °C. This level of temperature is over the melting limit of even lubricants with Extreme Pressure (EP) additives (critical temperature around 150 °C). In other words, the lubricant may experience zones of local melting and collapse, leaving the cooperating surfaces unprotected.

It is then understood that the modelling of thermal effects is essential in any algorithm before more accurate conclusions can be drawn. However, it is recognised in the literature that the behaviour of lubricants at high pressures and temperatures has yet to be accurately explained and modelled. It is now widely speculated that, under high pressure, lubricants act like low modulus solids and this regime of state is

characterised as “glassy”. This effect will be further discussed later in the section dealing with the non-Newtonian behaviour of lubricants.

Because of time limitations of the current project, it was decided that lubricant thermal effects will be left out from the developing model. In doing this, it is recognised that the calculated film thickness will be slightly overestimated. This in turn will result in reduced roughness asperity interactions and, thus, smoother loading of the cooperating surfaces. However, it is understood that in the frame of the accuracy of the developed computer model, these effects are of secondary importance for fatigue life calculations and more important when aiming for more accurate traction modelling, i.e. when calculating the traction coefficient of the CVT (which is not the primary target of this project). Thermal effects *will* be incorporated in a future extension of the present model when traction calculations are of importance.

2.2 Thermal stresses from asperity interactions

Roughness asperities that collide to each other during the sliding motion of the cooperating surfaces of a CVT, result in local frictional heating. The produced heat is of a transient nature and dissipates (mainly) by conduction into the solids (roller and toroidal disk) of the CVT, raising the local temperature. These flash temperature events are of a very short duration (usually less than one thousandth of a second). Nevertheless, they still give rise to local thermal stresses.

Compared with mechanical stresses from a normal and tangential loading, thermal stresses have a much shorter range of action but a much higher magnitude. Their effects therefore are localised very close to the surfaces. It was found in Nikas (1999) that in the case of a surface heat source in the shape of a disk, the thermal stress effect disappears at a depth equal to the radius of the disk. Applying this conclusion for a heat source the size of a roughness asperity with a base of 4 microns in diameter, the effective depth of thermal influence from this asperity is 1-2 microns below the surface.

These effects may become important when the CVT is operating in the partial or boundary lubrication regime, i.e. when the lubricant film is not thick enough to

prevent the large majority of asperity interactions. For the model of the current project, asperity interactions are accounted for by means of an effective local tangential loading between interacting asperities, based on the calculated local pressure and an assumed friction coefficient for boundary lubrication (usually 0.06). Thermal stresses from asperity interactions are ignored and may form part of a future extension of the current project.

The exclusion of asperity thermal stressing from the present model is expected to result in a slight overestimation of the life expectancy of the CVT, but only when the CVT is working at very low lambda ratios (lambda ratio < 1-2) for long periods of time during its operational life. However, considering the number of different factors already incorporated in the current version of the model, it is believed that the omission of asperity thermal effects is justified and will not yield unrealistic CVT fatigue life results.

2.3 Lubricant non-Newtonian effects

A typical contact of a CVT is a sliding/spinning contact. There is usually a significant amount of sliding, which means that the lubricant used experiences high shear rates. Moreover, the contact is usually under high fluid pressures (pressures over 1 GPa). High pressures and shear strain rates result in non-Newtonian behaviour of the lubricant, i.e. the relationship between the shear strain rate and the shear stress in the lubricant is not linear as it is assumed for Newtonian behaviour.

Furthermore, there is now substantial experimental evidence in the literature that beyond a certain pressure and temperature, the shear stress no longer increases with the shear strain rate in the lubricant and the lubricant behaves like a low modulus plastic solid (“glassy” state). The critical value of the shear stress when this behaviour commences is named “limiting shear stress”. The accurate value of this limiting shear stress is of great significance for traction calculations in CVTs because, as is shown later in this report, most of the contact is operating under this limiting-shear-stress regime.

The model developed for this project accounts for both non-Newtonian effects and a limiting shear stress. As a matter of fact, the Reynolds equation developed for this particular CVT application is generalised in the sense that it allows the use of many different non-Newtonian laws to describe lubricant behaviour, all of which have the concept of a limiting shear stress implemented to them. It must be noted though that the differences between different non-Newtonian laws are not significant (as it came out from the results of this project) and the variety of choices offered to a designer/researcher does not lead to conflicting results.

2.4 Surface roughness effects

The working surfaces of the roller and the toroidal disk of a CVT are normally rough. In the case of a TOROTRAK variator, a typical RMS roughness value is 0.2 μm . Roughness asperities are known to produce lubricant pressure ripples and are normally elastically flattened to a significant extent when subjected to the high elastohydrodynamic pressures encountered in typical CVT contacts. Pressure ripples (variations) are vital in any fatigue life model as it is normally these irregularities that govern the onset and propagation of cracks that lead to spalling (fatigue failure). It is therefore essential for any computational model to account for these effects, especially when combined with the observations of § 2.2.

As a result, the present model allows for any 3-dimensional surface profile to be used, either be it artificially created or measured experimentally. As an added benefit of using real (experimentally measured) rough surface profiles, any surface defects (bumps, debris dents etc) can be used in the analysis and their effect on fatigue life be evaluated.

2.5 Transient effects

During the operation of a CVT, rapid changes of the transmitted load are normally expected, owing to the ever changing demands for torque or speed. Such load changes may be accompanied by changes in the spinning speeds of the roller and the toroidal disk, and also the working angle between the roller and the toroidal disk, the latter inferring changes in the geometrical parameters (radii of curvature) at the area of the contact. All these effects are transient and often random in nature. For example, when the CVT is used on a road vehicle, the operation load (torque) is decided by the demands of the driver of the vehicle and, although a CVT can be pre-programmed to act as a manual gearbox with specific (predetermined) gear ratios, in general, “gear (ratio) changes” still consist a transient action.

For a realistic simulation of the operation of a CVT, transient effects must be modelled by means of a representative series of “actions”, i.e. a set of transmitted loads and accompanying contact geometries and velocities that form a representative scenario of the real-life operation of the CVT. The model of this project allows the designer to give a series of working conditions (loads, surface speeds and radii of curvature) taken from measurements during the operation of a CVT, as a means of a realistic simulation. Undoubtedly, fatigue life calculations can be performed even for a constant load/geometry/speed scenario, but that would be unrealistic and could yield misleading results, namely either an overestimation or even an underestimation of the fatigue life. For the sake of a relatively fast calculation of the fatigue life, a constant load/speed/geometry can be used, but for more accurate predictions, a real working example should be tested.

3. Solution of the lubrication problem

This section is devoted to the development of a generalised form of the Reynolds equation that describes the lubrication of a concentrated contact. The analysis is generalised in the sense that it allows the use of any non-Newtonian law to be used in the Reynolds equation without any modifications. A similar analysis was presented by Yang and Wen (1990a).

3.1 Development of a generalised lubrication equation

Figure 3.1 shows a fluid element in contact with the cooperating surfaces of a lubricated contact.

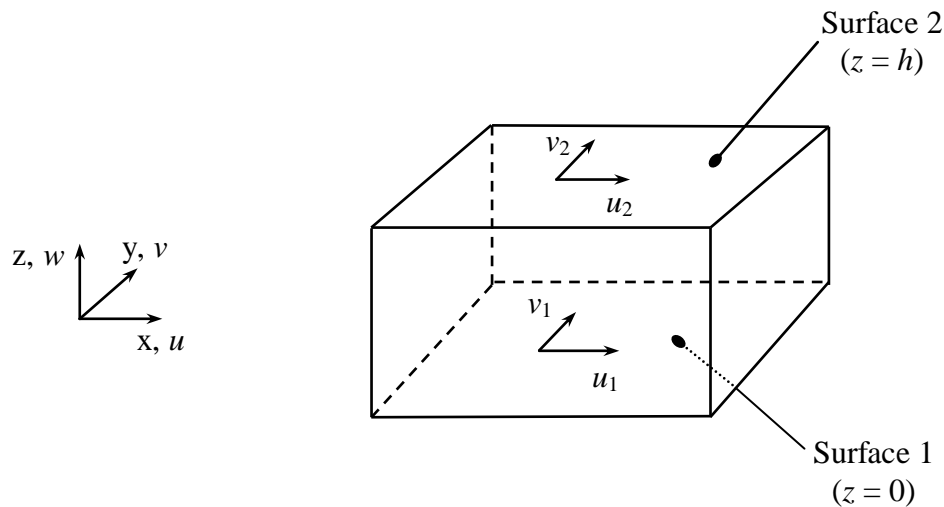


Figure 3.1 Fluid element in contact with the cooperating surfaces in a EHL contact.

From the force equilibrium on the fluid element, the following two equations are derived.

$$\frac{\partial p}{\partial x} = \frac{\partial \tau_{zx}}{\partial z} \quad , \quad \frac{\partial p}{\partial y} = \frac{\partial \tau_{zy}}{\partial z} \quad (3.1)$$

where p is the fluid pressure, which is constant across the film, and τ_{zx} and τ_{zy} are the viscous shear stresses on the fluid element, given by

$$\tau_{zx} = \eta_x \cdot \frac{\partial u}{\partial z} \quad , \quad \tau_{zy} = \eta_y \cdot \frac{\partial v}{\partial z} \quad (3.2)$$

where u and v are the tangential velocities of the counterfaces (shown in figure 3.1), and η_x and η_y denote the equivalent viscosity in direction x and y respectively. This equivalent viscosity formulation allows the incorporation of any non-Newtonian model, as is shown later. For a Newtonian fluid, the equivalent viscosity is equal to the usual dynamic viscosity.

Using equations (3.1), equations (3.2) yield:

$$\frac{\partial p}{\partial x} = \frac{\partial}{\partial z} \left(\eta_x \cdot \frac{\partial u}{\partial z} \right) \quad , \quad \frac{\partial p}{\partial y} = \frac{\partial}{\partial z} \left(\eta_y \cdot \frac{\partial v}{\partial z} \right) \quad (3.3)$$

Integrating the first of equations (3.3) twice with regard to z gives

$$\frac{\partial p}{\partial x} \cdot \int_0^z \frac{z'}{\eta_x} \cdot dz' = u + A_1(x, y, t) \cdot \int_0^z \frac{1}{n_x} \cdot dz' + A_2(x, y, t) \quad (3.4)$$

where A_1 and A_2 are integration functions of the spatial variables x and y , as well as of time t . Assuming the classical zero-slip condition holds at the solid-fluid interface, the following velocity boundary conditions apply.

$$\left. \begin{array}{l} \text{For } z = 0: \quad u = u_1, v = v_1, w = w_1 \\ \text{For } z = h: \quad u = u_2, v = v_2, w = w_2 \end{array} \right\} \quad (3.5)$$

Using the first condition (3.5) (for $z = 0$), integration functions A_1 and A_2 can easily be found:

$$A_1(x, y, t) = \frac{u_1 - u_2 + \frac{\partial p}{\partial x} \cdot \int_0^h \frac{z}{\eta_x} \cdot dz}{\int_0^h \frac{1}{\eta_x} \cdot dz} \quad \text{and} \quad A_2(x, y, t) = -u_1 \quad (3.6)$$

where h is the thickness of the fluid element (figure 3.1). Taking A_1 and A_2 from equations (3.6), equations (3.4) give

$$u = u_1 + \frac{\partial p}{\partial x} \cdot \int_0^z \frac{z'}{\eta_x} \cdot dz' - \frac{u_1 - u_2 + \frac{\partial p}{\partial x} \cdot \int_0^h \frac{z}{\eta_x} \cdot dz}{\int_0^h \frac{1}{\eta_x} \cdot dz} \cdot \int_0^z \frac{1}{\eta_x} \cdot dz' \quad (3.7)$$

Similarly, fluid velocity v is given by

$$v = v_1 + \frac{\partial p}{\partial y} \cdot \int_0^z \frac{z'}{\eta_y} \cdot dz' - \frac{v_1 - v_2 + \frac{\partial p}{\partial y} \cdot \int_0^h \frac{z}{\eta_y} \cdot dz}{\int_0^h \frac{1}{\eta_y} \cdot dz} \cdot \int_0^z \frac{1}{\eta_y} \cdot dz' \quad (3.8)$$

In order to make the previous expressions more compact, the following functions are defined:

$$\left. \begin{aligned} c_{z,x}(z) &\equiv \int_0^z \frac{1}{\eta_x} \cdot dz' & , & & c_{z,y}(z) &\equiv \int_0^z \frac{1}{\eta_y} \cdot dz' \\ c_{zz,x}(z) &\equiv \int_0^z \frac{z'}{\eta_x} \cdot dz' & , & & c_{zz,y}(z) &\equiv \int_0^z \frac{z'}{\eta_y} \cdot dz' \end{aligned} \right\} \quad (3.9)$$

Using equations (3.9), equations (3.7) and (3.8) are simplified as follows:

$$\left. \begin{aligned} u &= u_1 + \left[c_{zz,x}(z) - \frac{c_{zz,x}(h)}{c_{z,x}(h)} \cdot c_{z,x}(z) \right] \cdot \frac{\partial p}{\partial x} + \frac{u_2 - u_1}{c_{z,x}(h)} \cdot c_{z,x}(z) \\ v &= v_1 + \left[c_{zz,y}(z) - \frac{c_{zz,y}(h)}{c_{z,y}(h)} \cdot c_{z,y}(z) \right] \cdot \frac{\partial p}{\partial y} + \frac{v_2 - v_1}{c_{z,y}(h)} \cdot c_{z,y}(z) \end{aligned} \right\} \quad (3.10)$$

Having found suitable equations to calculate the fluid velocities u and v , the continuity equation can now be applied:

$$\frac{\partial \rho}{\partial t} + \frac{\partial}{\partial x}(\rho \cdot u) + \frac{\partial}{\partial y}(\rho \cdot v) + \frac{\partial}{\partial z}(\rho \cdot w) = 0 \quad (3.11)$$

where ρ is the fluid density. Integrating the mass conservation equation (3.11) with respect to z between the two solid boundaries ($z = 0$ and $z = h$), the following equation is derived:

$$\int_0^h \frac{\partial \rho}{\partial t} \cdot dz + \int_0^h \frac{\partial}{\partial x}(\rho \cdot u) \cdot dz + \int_0^h \frac{\partial}{\partial y}(\rho \cdot v) \cdot dz + \int_0^h \frac{\partial}{\partial z}(\rho \cdot w) \cdot dz = 0 \quad (3.12)$$

From the mathematical analysis of multivariable functions, the following rule of integration is known for functions $f(x,y,z)$ that are continuous and have continuous partial derivatives:

$$\int_a^b \frac{\partial}{\partial x} f(x, y, z) \cdot dz = \frac{\partial}{\partial x} \left[\int_a^b f(x, y, z) \cdot dz \right] + f(x, y, a) \cdot \frac{\partial a}{\partial x} - f(x, y, b) \cdot \frac{\partial b}{\partial x} \quad (3.13)$$

Rule (3.13) is applied to the integral terms of equation (3.12) with the following results:

$$\left. \begin{aligned}
 \int_0^h \frac{\partial \rho}{\partial t} \cdot dz &= \frac{\partial}{\partial t} \left(\int_0^h \rho \cdot dz \right) - \rho_2 \cdot \frac{\partial h}{\partial t} \\
 \int_0^h \frac{\partial}{\partial x} (\rho \cdot u) \cdot dz &= \frac{\partial}{\partial x} \left(\int_0^h \rho \cdot u \cdot dz \right) - \rho_2 \cdot u_2 \cdot \frac{\partial h}{\partial x} \\
 \int_0^h \frac{\partial}{\partial y} (\rho \cdot v) \cdot dz &= \frac{\partial}{\partial y} \left(\int_0^h \rho \cdot v \cdot dz \right) - \rho_2 \cdot v_2 \cdot \frac{\partial h}{\partial y} \\
 \int_0^h \frac{\partial}{\partial z} (\rho \cdot w) \cdot dz &= \rho_2 \cdot w_2 - \rho_1 \cdot w_1
 \end{aligned} \right\} \quad (3.14)$$

The film thickness h is a function of space and time, i.e. $h = h(x, y, t)$. Therefore, the total derivative of h is

$$dh = \frac{\partial h}{\partial x} \cdot dx + \frac{\partial h}{\partial y} \cdot dy + \frac{\partial h}{\partial t} \cdot dt \quad (3.15)$$

Equation (3.15) further gives:

$$\underbrace{\frac{dh}{dt}}_w = \frac{\partial h}{\partial x} \cdot \underbrace{\frac{dx}{dt}}_u + \frac{\partial h}{\partial y} \cdot \underbrace{\frac{dy}{dt}}_v + \frac{\partial h}{\partial t} \Rightarrow w = \frac{\partial h}{\partial x} \cdot u + \frac{\partial h}{\partial y} \cdot v + \frac{\partial h}{\partial t} \quad (3.16)$$

Using equations (3.14) and (3.15) in (3.13), the result is

$$\frac{\partial}{\partial t} \left(\int_0^h \rho \cdot dz \right) + \frac{\partial}{\partial x} \left(\int_0^h \rho \cdot u \cdot dz \right) + \frac{\partial}{\partial y} \left(\int_0^h \rho \cdot v \cdot dz \right) = 0 \quad (3.17)$$

Fluid velocities u and v are now taken from equations (3.7) and (3.8) and used in the relative integral terms of equation (3.17):

$$\left. \begin{aligned} \int_0^h \rho \cdot u \cdot dz &= d \cdot u_1 + \left[d_{zz,x} - \frac{c_{zz,x}(h)}{c_{z,x}(h)} \cdot d_{z,x} \right] \cdot \frac{\partial p}{\partial x} + \frac{u_2 - u_1}{c_{z,x}(h)} \cdot d_{z,x} \\ \int_0^h \rho \cdot v \cdot dz &= d \cdot v_1 + \left[d_{zz,y} - \frac{c_{zz,y}(h)}{c_{z,y}(h)} \cdot d_{z,y} \right] \cdot \frac{\partial p}{\partial y} + \frac{v_2 - v_1}{c_{z,y}(h)} \cdot d_{z,y} \end{aligned} \right\} \quad (3.18)$$

where

$$\left. \begin{aligned} d &\equiv \int_0^h \rho \cdot dz \\ d_{z,x} &\equiv \int_0^h \rho \cdot c_{z,x}(z) \cdot dz \quad , \quad d_{z,y} \equiv \int_0^h \rho \cdot c_{z,y}(z) \cdot dz \\ d_{zz,x} &\equiv \int_0^h \rho \cdot c_{zz,x}(z) \cdot dz \quad , \quad d_{zz,y} \equiv \int_0^h \rho \cdot c_{zz,y}(z) \cdot dz \end{aligned} \right\} \quad (3.19)$$

Finally, using equations (3.18) in (3.17), the lubrication equation is derived:

$$\begin{aligned} \frac{\partial d}{\partial t} + \frac{\partial}{\partial x} \left\{ d \cdot u_1 + \left[d_{zz,x} - \frac{c_{zz,x}(h)}{c_{z,x}(h)} \cdot d_{z,x} \right] \cdot \frac{\partial p}{\partial x} + \frac{u_2 - u_1}{c_{z,x}(h)} \cdot d_{z,x} \right\} + \\ \frac{\partial}{\partial y} \left\{ d \cdot v_1 + \left[d_{zz,y} - \frac{c_{zz,y}(h)}{c_{z,y}(h)} \cdot d_{z,y} \right] \cdot \frac{\partial p}{\partial y} + \frac{v_2 - v_1}{c_{z,y}(h)} \cdot d_{z,y} \right\} = 0 \end{aligned} \quad (3.20)$$

Equation (3.20) is a generalised form of the Reynolds equation for transient, rough, non-Newtonian elastohydrodynamic lubrication problems. In essence, this equation relates the fluid pressure and the film thickness in a lubricated contact. The generalised treatment of lubricant rheology models is presented in the next section.

3.2 Lubricant rheology models

In the classical Newtonian approach, the relation between the shear stress τ and shear strain rate s between two adjacent lubricant layers is assumed linear. However, as was explained earlier, for high fluid pressures and shear strain rates, this relationship becomes non-linear. Therefore, treating a traction fluid - that must serve CVT contacts under extreme working conditions - as Newtonian is not accurate. The development of a generalised lubrication equation in § 3.1 served precisely this purpose: to allow the application of virtually any rheology model in the CVT model and give the designer/researcher freedom of choice for experimentation. The computer code written for this project has a number of pre-programmed rheology models, all of which are presented below. According to the notation used, the shear stress is $\tau = \tau_{zx}$ or $\tau = \tau_{zy}$, whereas the shear strain rate is $s = \partial u/\partial z$ or $s = \partial v/\partial z$. For a more realistic approach, the concept of a limiting shear stress (discussed in § 3.3) was used even in the Newtonian model, which, originally, did not have any limitation.

Integrating equations (3.1) with respect to z , yields:

$$\tau_{zx} = \tau_{zx}^{(i)} + z \cdot \frac{\partial p}{\partial x} \quad , \quad \tau_{zy} = \tau_{zy}^{(i)} + z \cdot \frac{\partial p}{\partial y} \quad (3.21)$$

Equations (3.21) are needed in the numerical solution of the lubrication equation, when the non-Newtonian rheology models are used, as is shown later.

3.2.1 Newtonian rheology model and lubricant viscosity

This model is valid only for relatively low pressures and shear strain rates. The relation between fluid internal shear stress τ and shear strain rate s is linear:

$$\tau = \eta \cdot s \quad (3.22)$$

where η represents the dynamic viscosity of the fluid, which, generally, depends on the pressure and temperature of the fluid.

There are two widely used formulas in the literature, that give the dynamic viscosity of a fluid: the one proposed by Barus (1893) and the one proposed by Roelands (1966). The classical Barus' formula reads as follows:

$$\eta = \eta_0 \cdot e^{\alpha \cdot p} \quad (3.23)$$

where η_0 is the absolute viscosity at $p = 0$ (ambient pressure) and at a constant (representative) temperature, and α is the pressure-viscosity coefficient of the lubricant, which depends on the temperature. It has been experimentally found that for most lubricants, equation (3.23) gives acceptable results for pressures up to 0.1 GPa and becomes progressively inaccurate for higher pressures. For the large majority of lubricants, equation (3.23) gives unacceptably high viscosity for pressure over 1 GPa and, incidentally, that is the range of operation of heavily loaded contacts, as are those in a CVT. A generally better equation was proposed by Roelands (1966) after a lot of experimental work. Roelands' semi-empirical formula, which additionally accounts readily for the effect of temperature on the viscosity, reads as follows (SI units only):

$$\eta = \eta_0 \cdot \exp \left\{ \left[\ln(\eta_0) + 9.67 \right] \cdot \left[\left(1 + 5.1 \cdot 10^{-9} \cdot p \right)^{Z_1} \cdot \left(\frac{\theta - 138}{\theta_0 - 138} \right)^{-S_0} - 1 \right] \right\} \quad (\text{SI units}) \quad (3.24)$$

where Z_1 and S_0 are the viscosity-pressure and viscosity-temperature coefficients respectively, θ is the lubricant temperature and θ_0 is the environmental temperature (temperatures in degrees Kelvin, pressure in Pa and viscosity in Pa·s).

Constants Z_1 and α of the Roelands' and Barus' equations can be related through Houpert's formula, derived by the fact that Roelands' and Barus' formulas must give the same viscosity as the pressure tends to zero:

$$Z_1 = \frac{\alpha}{5.1 \cdot 10^{-9} \cdot [\ln(\eta_0) + 9.67]} \quad (\text{SI units}) \quad (3.25)$$

Equations (3.23) and (3.24) agree well for low pressures but deviate substantially for pressures over 1 GPa (the difference in the viscosity calculated from (3.23) and from (3.24) could be several orders of magnitude, depending on the

lubricant – see for example Hamrock, 1994, figure 4.4). However, there are some traction fluids (for example Santotrac 50) which, apparently, show a better agreement with Barus' model, even for high pressures. Since traction fluids is the choice for CVTs, the model of this project allows both Barus' and Roelands' equations to be used. Moreover, due to the omission of thermal effects in the current version of the CVT model, as is explained in § 2.1, a representative (operation) temperature is chosen whenever the Roelands' formula is used instead of a (calculated) local lubricant temperature (which normally varies in the contact).

3.2.2 Bair and Winner (1979) rheology model

According to this model, the relation between the fluid internal shear stress τ and shear strain rate s is

$$s = \frac{-\tau_L}{\eta} \cdot \ln\left(1 - \frac{\tau}{\tau_L}\right) \quad (3.26)$$

where τ_L is the limiting shear stress (see § 3.3). From equation (3.26), two equations are derived for directions x and y:

$$\frac{\partial u}{\partial z} = \frac{-\tau_L}{\eta} \cdot \ln\left(1 - \frac{\tau_{zx}}{\tau_L}\right) \quad , \quad \frac{\partial v}{\partial z} = \frac{-\tau_L}{\eta} \cdot \ln\left(1 - \frac{\tau_{zy}}{\tau_L}\right) \quad (3.27)$$

Integrating equations (3.27) with respect to z across the film thickness and using equations (3.21), the following results are obtained:

$$\left. \begin{aligned} \int_0^h \frac{1}{\eta} \cdot \ln\left[1 - \frac{1}{\tau_L} \cdot \left(\tau_{zx}^{(1)} + z \cdot \frac{\partial p}{\partial x}\right)\right] \cdot dz &= \frac{u_1 - u_2}{\tau_L} \\ \int_0^h \frac{1}{\eta} \cdot \ln\left[1 - \frac{1}{\tau_L} \cdot \left(\tau_{zy}^{(1)} + z \cdot \frac{\partial p}{\partial y}\right)\right] \cdot dz &= \frac{v_1 - v_2}{\tau_L} \end{aligned} \right\} \quad (3.28)$$

Numerical solution of equations (3.28) yields the unknown shear stresses

$\tau_{zx}^{(1)}$ and $\tau_{zy}^{(1)}$ ($0 \leq \tau_{zx}^{(1)}, \tau_{zy}^{(1)} \leq \tau_L$), which can then be used in equations (3.21) to calculate the shear stresses at any position across the lubricant film.

3.2.3 Gecim and Winner (1980) rheology model

According to this model, the relation between the fluid internal shear stress τ and shear strain rate s is

$$s = \frac{\tau_L}{\eta} \cdot \operatorname{arctan} h \left(\frac{\tau}{\tau_L} \right) \quad (3.29)$$

From equations (3.29), two equations are derived for directions x and y:

$$\frac{\partial u}{\partial z} = \frac{\tau_L}{\eta} \cdot \operatorname{arctan} h \left(\frac{\tau_{zx}}{\tau_L} \right) \quad , \quad \frac{\partial v}{\partial z} = \frac{\tau_L}{\eta} \cdot \operatorname{arctan} h \left(\frac{\tau_{zy}}{\tau_L} \right) \quad (3.30)$$

Integrating equations (3.30) with respect to z across the film thickness and using equations (3.21), the following results are obtained:

$$\left. \begin{aligned} \int_0^h \frac{1}{\eta} \cdot \ln \left(\frac{\tau_L + z \cdot \frac{\partial p}{\partial x} + \tau_{zx}^{(1)}}{\tau_L - z \cdot \frac{\partial p}{\partial x} - \tau_{zx}^{(1)}} \right) \cdot dz &= \frac{2 \cdot (u_2 - u_1)}{\tau_L} \\ \int_0^h \frac{1}{\eta} \cdot \ln \left(\frac{\tau_L + z \cdot \frac{\partial p}{\partial y} + \tau_{zy}^{(1)}}{\tau_L - z \cdot \frac{\partial p}{\partial y} - \tau_{zy}^{(1)}} \right) \cdot dz &= \frac{2 \cdot (v_2 - v_1)}{\tau_L} \end{aligned} \right\} \quad (3.31)$$

Numerical solution of equations (3.31) yields the unknown shear stresses

$\tau_{zx}^{(1)}$ and $\tau_{zy}^{(1)}$ ($0 \leq \tau_{zx}^{(1)}, \tau_{zy}^{(1)} \leq \tau_L$), which can then be used in equations (3.21) to calculate the shear stresses at any position across the lubricant film.

3.2.4 Elsharkawy and Hamrock (1991) rheology model (“General” model)

According to this model, the relation between the fluid internal shear stress τ and shear strain rate s is

$$s = \frac{\frac{\tau}{\eta}}{\left[1 - \left(\frac{\tau}{\tau_L}\right)^\Lambda\right]^{1/\Lambda}} \quad (3.32)$$

where Λ is a parameter of the model that can take positive integer values ($\Lambda \geq 1$). For $\Lambda = 2$, the above model is identical to the Lee and Hamrock’s (1990a, 1990b) model, known as “circular” model. For $\Lambda > 2$, the Elsharkawy and Hamrock model behaves like other non-linear models and this is the reason why it is characterised as “general” model.

From equations (3.32), two equations are derived for directions x and y:

$$\frac{\partial u}{\partial z} = \frac{\frac{\tau_{zx}}{\eta}}{\left[1 - \left(\frac{\tau_{zx}}{\tau_L}\right)^\Lambda\right]^{1/\Lambda}}, \quad \frac{\partial v}{\partial z} = \frac{\frac{\tau_{zy}}{\eta}}{\left[1 - \left(\frac{\tau_{zy}}{\tau_L}\right)^\Lambda\right]^{1/\Lambda}} \quad (3.33)$$

Integrating equations (3.33) with respect to z across the film and using equations (3.21), the following results are obtained:

$$\left. \begin{aligned} \int_0^h \frac{\tau_{zx}^{(i)} + z \cdot \frac{\partial p}{\partial x}}{\eta \cdot \left\{1 - \left[\frac{1}{\tau_L} \cdot \left(\tau_{zx}^{(i)} + z \cdot \frac{\partial p}{\partial x}\right)\right]^\Lambda\right\}^{1/\Lambda}} \cdot dz = u_2 - u_1 \\ \int_0^h \frac{\tau_{zy}^{(i)} + z \cdot \frac{\partial p}{\partial y}}{\eta \cdot \left\{1 - \left[\frac{1}{\tau_L} \cdot \left(\tau_{zy}^{(i)} + z \cdot \frac{\partial p}{\partial y}\right)\right]^\Lambda\right\}^{1/\Lambda}} \cdot dz = v_2 - v_1 \end{aligned} \right\} \quad (3.34)$$

Numerical solution of equations (3.34) yields the unknown shear stresses

$\tau_{zx}^{(1)}$ and $\tau_{zy}^{(1)}$ ($0 \leq \tau_{zx}^{(1)}, \tau_{zy}^{(1)} \leq \tau_L$), which can then be used in equations (3.21) to calculate the shear stresses at any position across the lubricant film.

3.3 Lubricant limiting shear stress

It is now generally accepted that the lubricant internal shear stress does not increase indefinitely with increasing shear strain rate, but there is a lubricant-dependent critical value (limiting shear stress) that can not be exceeded (see for example Bair and Winer (1979), Hamrock (1994, § 4.15)). When the limiting shear stress is reached, the lubricant shears plastically with no further increase of the shear stress for increasing shear strain rate. Generally, the limiting shear stress τ_L is a function of lubricant pressure and temperature:

$$\tau_L = \tau_0 + \gamma \cdot p - \delta \cdot \theta \quad (3.35)$$

where constants τ_0 , γ and δ depend on the lubricant. For Santotrac 50 traction fluid (used in TOROTRAK CVTs), the constants in the limiting shear stress function are: $\tau_0 = 3.17 \cdot 10^7$ Pa, $\gamma = 0.093$ and $\delta = 317000$ Pa/°C (pressure p and shear stress τ_L in Pa, temperature θ in degrees Celsius).

3.4 Lubricant shear stress components

As is explained in § 3.3, the lubricant shear stress τ cannot exceed the limiting shear stress τ_L . So far, the mathematical analysis is based on using the two components of the shear stress τ , namely τ_{zx} and τ_{zy} ($\tau = \sqrt{\tau_{zx}^2 + \tau_{zy}^2}$). Questions arise when any (or both) of the calculated shear stress components approach the limiting shear stress, on how the resultant shear stress is divided into the two (x and y) components.

The constraint that must be satisfied is: $\tau_{zx}^2 + \tau_{zy}^2 \leq \tau_L^2$. From physical experience it is known that it is easier to remove a cork from a wine bottle by pulling and rotating it at the same time than by just pulling it. The same principle applies in the present case: when the shear strength of the lubricant is reached, the shear stress can no longer increase but, instead, *it changes direction* (see for example Jacobson *et al.*, 1987). Let's assume now that the calculated shear stress components violate the limiting shear stress constraint, i.e. $\tau_{zx}^2 + \tau_{zy}^2 > \tau_L^2$. This problem is resolved as follows:

- **Case $u > v$ (and $|\tau^{(\text{calculated})}| > \tau_L$)**

If $|\tau_{zx}^{(\text{calculated d})}| > \tau_L$, then set $\tau_{zx}^{(\text{new})} = \text{sgn}(\tau_{zx}^{(\text{calculated d})}) \cdot \tau_L$ (where $\text{sgn}(x)$ is the sign function of x ; $\text{sgn}(x) = +1$ if $x > 0$ and $\text{sgn}(x) = -1$ if $x < 0$) and $\tau_{zy}^{(\text{new})} = 0$.

Otherwise, if $|\tau_{zx}^{(\text{calculated d})}| < \tau_L$, then set $\tau_{zy}^{(\text{new})} = \text{sgn}(\tau_{zy}^{(\text{calculated d})}) \cdot \sqrt{\tau_L^2 - (\tau_{zx}^{(\text{calculated d})})^2}$ and $\tau_{zx}^{(\text{new})} = \tau_{zx}^{(\text{calculated d})}$.

- **Case $u < v$ (and $|\tau^{(\text{calculated})}| > \tau_L$)**

If $|\tau_{zy}^{(\text{calculated d})}| > \tau_L$, then set $\tau_{zy}^{(\text{new})} = \text{sgn}(\tau_{zy}^{(\text{calculated d})}) \cdot \tau_L$ and $\tau_{zx}^{(\text{new})} = 0$. Otherwise, if

$|\tau_{zy}^{(\text{calculated d})}| < \tau_L$, then set $\tau_{zx}^{(\text{new})} = \text{sgn}(\tau_{zx}^{(\text{calculated d})}) \cdot \sqrt{\tau_L^2 - (\tau_{zy}^{(\text{calculated d})})^2}$ and

$\tau_{zy}^{(\text{new})} = \tau_{zy}^{(\text{calculated d})}$.

- **Case $u = v$ (and $|\tau^{(\text{calculated})}| > \tau_L$)**

In this hypothetical scenario, it is assumed that the shear stress components must

be equal, thus: $\tau_{zx}^{(\text{new})} = \text{sgn}(\tau_{zx}^{(\text{calculate d})}) \cdot \frac{\tau_L}{\sqrt{2}}$ and $\tau_{zy}^{(\text{new})} = \text{sgn}(\tau_{zy}^{(\text{calculate d})}) \cdot \frac{\tau_L}{\sqrt{2}}$.

3.5 Lubricant density

The density of a lubricant is generally a function of pressure and temperature. From the original (1966) formula of Dowson and Higginson, which accounted only for the effect of pressure on the lubricant density (for pressures up to 0.4 GPa), a widely accepted generalisation, which is also used in the present CVT model, is the following semi-empirical formula (see for example Zhu and Wen, 1984):

$$\rho = \rho_0 \cdot \left[1 + \frac{c_1 \cdot P}{1 + c_2 \cdot p} - c_3 \cdot (\theta - \theta_0) \right] \quad (3.36)$$

where ρ_0 is the density at ambient conditions (zero pressure and environmental temperature), and c_1 , c_2 , c_3 are constants, depending on the fluid. For mineral oils, a typical set of constants is: $c_1 = 6 \cdot 10^{-10} \text{ Pa}^{-1}$, $c_2 = 17 \cdot 10^{-10} \text{ Pa}^{-1}$ and $c_3 = 65 \cdot 10^{-5} \text{ }^\circ\text{C}^{-1}$ (constants c_1 and c_2 are the same as those proposed by Dowson and Higginson in their original formula, which is derived from (3.36) by setting $c_3 = 0$). Also, a typical value for the ambient density for mineral oils is $\rho_0 = 870 \text{ kg/m}^3$.

If the effect of temperature is ignored, the maximum density increase for mineral oils is about 35 %, for pressures up to 2 GPa. However, at high pressure the lubricant is expected to change phase from liquid to solid. Hamrock (1994, § 4.14) suggests a formula where the solidification pressure of a lubricant is taken into account. Unfortunately, his approach does not account for the effect of temperature and requires five constants to be known before any calculations can be performed. Furthermore, the extremely high rate of pressure increase in a typical EHD contact is difficult to be experimentally replicated and evaluated in terms of a solidification pressure, because the phase change is extremely fast. As an example, a typical CVT

contact with a mean Hertzian contact radius of 500 μm , maximum lubricant pressure of 2 GPa, and sliding speed of 3 m/s, means that the pressure rises from zero to 2 GPa in $(500 \mu\text{m})/(3 \cdot 10^6 \mu\text{m/s}) = 0.17 \text{ ms}$, i.e. a rate of $1.2 \cdot 10^{13} \text{ Pa/s}$! At these rates, other phenomena must be accounted for, as for example the lubricant structural relaxation time.

More recently, Wong *et al.* (1996) proposed a different method to calculate lubricant density, based on the van der Waals equation of state. Their results showed good agreement with experiments for a pressure range 0.2-0.9 GPa. However, based on the arguments listed previously, equation (3.36) is still preferable for quick and sufficiently accurate calculations and, hence, is used in the present CVT model.

3.6 Geometry of the contact

Generally, the contact between a roller and a toroidal disk of a CVT variator is elliptical. The lengths of the axes of the contact ellipse can be calculated if it assumed that the real pressure distribution is approximated by an semi-ellipsoidal (Hertzian) distribution $p = p_0 \cdot [1 - (x/D_x)^2 + (y/D_y)^2]^{1/2}$, where D_x and D_y are the lengths of the semi-axes of the contact ellipse in axes x and y, respectively, and p_0 is the maximum Hertzian pressure.

At the area of contact, the undeformed surfaces of the roller and the toroidal disk of a CVT variator can be approximated by ellipsoids, having radii of curvature $r_x^{(\text{roller})}, r_y^{(\text{roller})}$ (roller) and $r_x^{(\text{disk})}, r_y^{(\text{disk})}$ (toroidal disk) in axes x and y. The following effective radii of curvature are now defined:

$$R_x \equiv \frac{r_x^{(\text{roller})} \cdot r_x^{(\text{disk})}}{r_x^{(\text{roller})} + r_x^{(\text{disk})}} \quad , \quad R_y \equiv \frac{r_y^{(\text{roller})} \cdot r_y^{(\text{disk})}}{r_y^{(\text{roller})} + r_y^{(\text{disk})}} \quad (3.37)$$

Following Johnson (1985, page 95) and assuming that the major contact ellipse axis lies along the x-axis, the effective radii of curvature and the contact ellipse semi-axes lengths satisfy the following equation:

$$\frac{R_x}{R_y} = \frac{\left(\frac{D_x}{D_y}\right)^2 \cdot E(e) - K(e)}{K(e) - E(e)} \quad , (D_x > D_y) \quad (3.38)$$

where

$$e \equiv \sqrt{1 - \left(\frac{D_y}{D_x}\right)^2} \quad , (D_x > D_y) \quad (3.39)$$

and $K(e)$ and $E(e)$ are the complete elliptic integrals of the 1st and 2nd kind of argument e , respectively:

$$K(e) \equiv \int_0^{\pi/2} \frac{1}{\sqrt{1 - e^2 \cdot \sin^2(\vartheta)}} \cdot d\vartheta \quad , \quad E(e) \equiv \int_0^{\pi/2} \sqrt{1 - e^2 \cdot \sin^2(\vartheta)} \cdot d\vartheta \quad (3.40)$$

Moreover, lengths D_x and D_y are related (see Johnson, 1985, equation (4.30)) as follows:

$$(D_x \cdot D_y)^{3/2} = \frac{3 \cdot P(t) \cdot \sqrt{R_x \cdot R_y}}{\pi \cdot E \cdot e^2} \cdot \left(\frac{D_y}{D_x}\right)^{3/2} \cdot \sqrt{\left[\left(\frac{D_x}{D_y}\right)^2 \cdot E(e) - K(e)\right] \cdot [K(e) - E(e)]} \quad (3.41)$$

where P is the load of the contact (assumed time-variable) and E is the effective modulus of elasticity

$$E \equiv \frac{1}{\frac{1 - \nu_{\text{roller}}^2}{E_{\text{roller}}} + \frac{1 - \nu_{\text{disk}}^2}{E_{\text{disk}}}} \quad (3.42)$$

where E_{roller} , E_{disk} are the moduli of elasticity of the roller and the toroidal disk, and ν_{roller} , ν_{disk} are the Poisson ratios. From equation (3.41), the length of the major semi-axis is derived:

$$D_x = \left\{ \frac{3 \cdot P(t) \cdot \sqrt{R_x \cdot R_y \cdot \left[\frac{E(e)}{1-e^2} - K(e) \right] \cdot [K(e) - E(e)]}}{\pi \cdot E \cdot e^2} \right\}^{1/3} \quad (3.43)$$

Then, from equation (3.39), the length of the semi-minor axis D_y is easily found:

$$D_y = D_x \cdot \sqrt{1-e^2} \quad (3.44)$$

In order to calculate D_x and D_y from equations (3.43) and (3.44), variable e must be calculated first. This is done by solving the non-linear equation (3.38) numerically. The same procedure is followed when the major axis of the contact ellipse lies along the y-axis ($D_y > D_x$). This method is used in the CVT analysis.

An alternative method is to use the formulas of Hamrock and Brewe (1983) for the approximation of the required elliptic integrals:

$$K \cong \frac{\pi}{2} + \left(\frac{\pi}{2} - 1 \right) \cdot \ln \left(\frac{R_x}{R_y} \right) \quad , \quad E \cong 1 + \left(\frac{\pi}{2} - 1 \right) \cdot \frac{R_y}{R_x} \quad , \quad (R_x > R_y) \quad (3.45)$$

Then D_x and D_y are calculated again from equations (3.43) and (3.44). This method is used for verification of the results obtained by the resolution of the non-linear equation (3.38). It was found that the two methods (accurate and approximate) agree very well.

3.7 Film thickness (geometry, roughness and elastic deformations)

The local film thickness in a lubricated contact depends on the local geometry of the cooperating lubricated surfaces, the surface roughness and the surface displacements due to the contact pressure:

$$\text{Film thickness} = \text{Constant} + \text{Geometry} + \text{Roughness} + \text{Displacements}$$

The geometry of the surfaces at the area of the “contact” is approximated by ellipsoids (see § 3.6 and equations (3.37)). In doing so, and assuming that the effective radii of curvature of the surfaces are R_x and R_y (equations (3.37)), the exact distance D between the two cooperating surfaces is

$$D(x, y) = R_x + R_y - \sqrt{R_x^2 - x^2} - \sqrt{R_y^2 - y^2} \quad (3.46)$$

where x and y are measured from the centre of the contact (0,0).

The combined surface roughness ζ is the sum of the roughness of each surface, ζ_{roller} and ζ_{disk} . However, in the case of asperity interactions, there is a significant probability of local deformation of individual asperities. If this happens, the roughness must be modified in real time. Therefore, the equation of the combined surface roughness ζ must allow for a term that accounts for any possible plastic deformations:

$$\zeta(x, y, t) = \zeta_{\text{roller}}(x, y) + \zeta_{\text{disk}}(x, y) + D_p(x, y, t) \quad (3.47)$$

where $D_p(x, y, t)$ gives the local plastic deformation of the surfaces, if there is one, and is discussed in § 4. (That plasticity term is actually used to study the change of surface topography in real time as the roller and the toroidal disk are kept engaged and rotating.) The roughness of each surface is considered as the distance of a surface point from a mean surface, the latter being the surface of the ellipsoid used to approximate the real surface at the area of the contact. Asperities have negative roughness whereas cavities have positive roughness, in the sense that asperities result in thinner films than when using a perfect ellipsoidal surface and, correspondingly, cavities result in thicker films. The CVT model in this report allows for real rough 2-d surface data to be used in the calculations.

The transient normal elastic displacements of the surfaces, owing to the pressure and traction distribution in the contact, are given by

$$D_e(x, y, t) = \iint_{\substack{\text{contact} \\ \text{ellipse}}} \left[\frac{p(\xi, \psi, t)}{\sqrt{(x-\xi)^2 + (y-\psi)^2}} + \frac{(\xi-x) \cdot \bar{\tau}_{zx}(\xi, \psi, t) + (\psi-y) \cdot \bar{\tau}_{zy}(\xi, \psi, t)}{(x-\xi)^2 + (y-\psi)^2} \right] \cdot d\xi \cdot d\psi \quad (3.48)$$

where the first fraction inside the above double integral accounts for the contribution of the normal pressure (p) to the normal displacements and the second fraction accounts for the contribution of the surface tractions ($\bar{\tau}_{zx}, \bar{\tau}_{zy}$).

The disadvantage of using equation (3.48) directly is the discontinuity of the integrated function at points ($x = \xi, y = \psi$), as well as the amount of CPU time needed to accurately evaluate the double integral (a process that must be repeated for, usually, hundreds or thousands of grid points at every time step and/or correction loop of a computation algorithm). Therefore, instead of numerically evaluating the double integral of equation (3.48), a much faster method is followed. Each surface is analysed in a number of elemental rectangles of dimensions $2 \cdot \Delta x$ and $2 \cdot \Delta y$. The normal elastic surface displacement at point (x, y) of a semi-infinite solid subjected to a pressure p at point (x_0, y_0) is (see for example Johnson, 1985, equation (3.22b)):

$$\bar{u}_z^{(p)}(x, y; x_0, y_0) = \frac{1-\nu^2}{\pi \cdot E} \cdot \frac{dx_0 \cdot dy_0 \cdot p}{\sqrt{(x-x_0)^2 + (y-y_0)^2}} \quad (3.49)$$

where E is the elastic modulus of the solid. The elastic surface displacement at a point (x, y) due to a uniform pressure over a rectangular area $2 \cdot \Delta x \times 2 \cdot \Delta y$ is then

$$\bar{u}_z^{(p)}(x, y) = \frac{(1-\nu^2) \cdot p}{\pi \cdot E} \cdot \int_{-\Delta x}^{\Delta x} \int_{-\Delta y}^{\Delta y} \frac{1}{\sqrt{(x-\xi)^2 + (y-\psi)^2}} \cdot d\xi \cdot d\psi \quad (3.50)$$

Performing the integration in equation (3.50) yields the following result:

$$\bar{u}_z^{(p)}(x, y) \cong \frac{1-\nu^2}{E} \cdot p \cdot \left\{ \begin{array}{l} (x + \Delta x) \cdot \ln \left[\frac{y + \Delta y + \sqrt{(y + \Delta y)^2 + (x + \Delta x)^2}}{y - \Delta y + \sqrt{(y - \Delta y)^2 + (x + \Delta x)^2}} \right] + \\ (y + \Delta y) \cdot \ln \left[\frac{x + \Delta x + \sqrt{(y + \Delta y)^2 + (x + \Delta x)^2}}{x - \Delta x + \sqrt{(y + \Delta y)^2 + (x - \Delta x)^2}} \right] + \\ (x - \Delta x) \cdot \ln \left[\frac{y - \Delta y + \sqrt{(y - \Delta y)^2 + (x - \Delta x)^2}}{y + \Delta y + \sqrt{(y + \Delta y)^2 + (x - \Delta x)^2}} \right] + \\ (y - \Delta y) \cdot \ln \left[\frac{x - \Delta x + \sqrt{(y - \Delta y)^2 + (x - \Delta x)^2}}{x + \Delta x + \sqrt{(y - \Delta y)^2 + (x + \Delta x)^2}} \right] \end{array} \right\} \quad (3.51)$$

Equation (3.51) is extremely useful for computer programming by taking $x = i \cdot \Delta x$ and $y = j \cdot \Delta y$. The surface normal displacement is then calculated through the use of influence coefficients C_{ijmn} (using tensor notation) as

$$\bar{u}_z \cong \sum_m \sum_n C_{ijmn} \cdot p_{mn} \quad , (m, n) \neq (i, j) \quad (3.52)$$

The influence coefficients are calculated only once and this saves an enormous amount of computing time.

Most engineering analyses stop at this point, i.e. the surface displacements are considered to be the result of the normal pressure p only. However, in heavily loaded contacts and especially contacts with (sometimes) a significant proportion of asperity interactions as in the case of a CVT, surface normal displacements are also affected by traction, be it elasto-hydrodynamically derived or of a solid-contact origin (asperity friction). For the sake of completeness, this influence must be accounted for. The author could not find an equation similar to (3.51) and, therefore, undertook the laborious task to produce one in the same manner that equation (3.51) was earlier proved. After a lot of algebraic work, the normal elastic surface displacement due a uniform traction $\bar{\tau}_{zx}$ over a rectangular area $2 \cdot \Delta x \times 2 \cdot \Delta y$ is calculated as follows:

$$\bar{u}_z^{(\bar{\tau}_{zx})} \cong \frac{(2 \cdot \nu - 1) \cdot (1 + \nu)}{2 \cdot \pi \cdot E} \cdot \bar{\tau}_{zx} \cdot \left\{ \begin{array}{l} (x - \Delta x) \cdot \left[\arctan\left(\frac{y + \Delta y}{x - \Delta x}\right) - \arctan\left(\frac{y - \Delta y}{x - \Delta x}\right) \right] + \\ (x + \Delta x) \cdot \left[\arctan\left(\frac{y - \Delta y}{x + \Delta x}\right) - \arctan\left(\frac{y + \Delta y}{x + \Delta x}\right) \right] + \\ \frac{1}{2} \cdot \left\{ \begin{array}{l} (y + \Delta y) \cdot \ln \left[\frac{(x - \Delta x)^2 + (y + \Delta y)^2}{(x + \Delta x)^2 + (y + \Delta y)^2} \right] - \\ (y - \Delta y) \cdot \ln \left[\frac{(x - \Delta x)^2 + (y - \Delta y)^2}{(x + \Delta x)^2 + (y - \Delta y)^2} \right] \end{array} \right\} \end{array} \right\} \quad (3.53)$$

Similarly, using a uniform traction $\bar{\tau}_{zy}$, the result is:

$$\bar{u}_z^{(\bar{\tau}_{zy})} \cong \frac{(2 \cdot \nu - 1) \cdot (1 + \nu)}{2 \cdot \pi \cdot E} \cdot \bar{\tau}_{zy} \cdot \left\{ \begin{array}{l} (y - \Delta y) \cdot \left[\arctan\left(\frac{x + \Delta x}{y - \Delta y}\right) - \arctan\left(\frac{x - \Delta x}{y - \Delta y}\right) \right] + \\ (y + \Delta y) \cdot \left[\arctan\left(\frac{x - \Delta x}{y + \Delta y}\right) - \arctan\left(\frac{x + \Delta x}{y + \Delta y}\right) \right] + \\ \frac{1}{2} \cdot \left\{ \begin{array}{l} (x + \Delta x) \cdot \ln \left[\frac{(x + \Delta x)^2 + (y - \Delta y)^2}{(x + \Delta x)^2 + (y + \Delta y)^2} \right] - \\ (x - \Delta x) \cdot \ln \left[\frac{(x - \Delta x)^2 + (y - \Delta y)^2}{(x - \Delta x)^2 + (y + \Delta y)^2} \right] \end{array} \right\} \end{array} \right\} \quad (3.54)$$

Finally, the transient normal elastic displacements of the surfaces, owing to the pressure and traction distribution in the contact, are calculated by superposition of the individual displacements for both solids (roller and toroidal disk of the CVT):

$$D_e(x, y, t) = \bar{u}_z^{(p(x,y,t))} + \bar{u}_z^{(\bar{\epsilon}_{zx}(x,y,t))} + \bar{u}_z^{(\bar{\epsilon}_{zy}(x,y,t))} \quad (3.55)$$

The film thickness equation can now be written as

$$h(x, y, t) = h(0,0,t) + D(x, y) + \zeta(x, y, t) + D_e(x, y, t) - D_e(0,0,t) \quad (3.56)$$

where the reference point for the surface displacements is the centre of the contact. Note that any plastic displacements (usually due to local asperity collisions) have already been included in the roughness term ζ (see equation (3.47)).

3.8 Boundary and other conditions

- The zero-slip boundary condition was introduced in equations (3.5), i.e. the fluid velocities at the fluid-solid interface are the tangential velocities of the counterfaces (roller and toroidal disk).
- It is assumed that the fluid pressure cannot become negative:

$$p(x, y, t) \geq 0 \quad (3.57)$$

Therefore, whenever a fluid pressure is calculated negative, it is set equal to zero.

- It is assumed that the contact operates in an environment without structural vibrations. Therefore, the supported load in the contact must be equal to the load that has to be transmitted (P):

$$\int_{-\infty}^{\infty} \int_{-\infty}^{\infty} p(x, y, t) = P(t) \quad (3.58)$$

Pressure p in equation (3.58) includes of course both fluid and, if any, solid pressure.

- At the areas of solid contact (if any), the shear stress is the product of the pressure and the boundary lubrication friction coefficient μ (usually $\mu = 0.06$)

$$h(x, y, t) = 0 \Rightarrow \left\{ \begin{array}{l} \bar{\tau}_{zx}^{(\text{roller})}(x, y, t) = \mu \cdot p(x, y, t) \cdot \text{sgn}(u_1(t) - u_2(t)), \bar{\tau}_{zx}^{(\text{disk})}(x, y, t) = -\bar{\tau}_{zx}^{(\text{roller})}(x, y, t) \\ \bar{\tau}_{zy}^{(\text{roller})}(x, y, t) = \mu \cdot p(x, y, t) \cdot \text{sgn}(v_1(t) - v_2(t)), \bar{\tau}_{zy}^{(\text{disk})}(x, y, t) = -\bar{\tau}_{zy}^{(\text{roller})}(x, y, t) \end{array} \right\} \quad (3.59)$$

- It is known that yield occurs when the surface pressure exceeds a limit of (approximately) $1.6 \cdot Y$, where Y is the yield stress in simple tension. If the calculated pressure at any point exceeds this plasticity limit, then that pressure is set equal to the plasticity limit:

$$\text{If } p^{(\text{calculated})}(x, y, t) > 1.6 \cdot Y \text{ then } p^{(\text{new})}(x, y, t) = 1.6 \cdot Y \quad (3.60)$$

4. Stress analysis

The typical contact in a TOROTRAK IVT variator is elliptical. The contact surface loading between a roller and a toroidal disk consists of normal pressure (p) and 2-dimensional surface tractions ($\bar{\tau}_{zx}, \bar{\tau}_{zy}$). Moreover, there may be thermal stresses due to roughness asperity collisions that produce frictional heat, as well as lubricant shear heating that results in heat being transferred to the cooperating surfaces, but these effects are not accounted for in the present study (a full thermoelastic analysis can be found in Nikas *et al.*, 1999). Based on the particular surface loading $\langle p, \bar{\tau}_{zx}, \bar{\tau}_{zy} \rangle$, the subsurface stress field in the roller and the toroidal disk can be calculated. To achieve this goal, the Boussinesq-Cerruti equations must be applied. These are the most general equations available and can be found in differential form in Johnson (1985). In order to be used in the calculations, the equations are further developed into more useful analytical relations. This task was undertaken by the author in his Doctoral thesis. Only the basic equations will be presented here.

The dimensions of a typical CVT contact are sufficiently small, compared with the main dimensions of the cooperating bodies (roller and toroidal disk), which justifies the consideration of the roller and the disk as two elastic half-spaces. Assuming surface A is one of two half-spaces, figure 4.1 shows surface A together with the coordinate system notation as well as the surface pressure and tractions, which comprise the boundary loading.

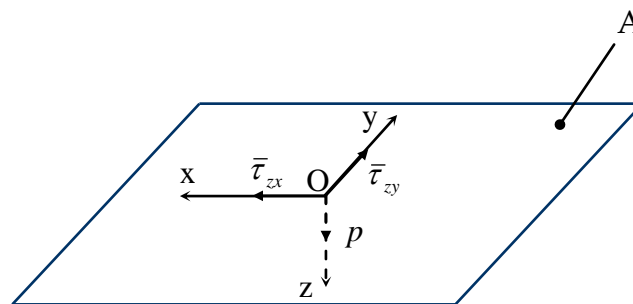


Figure 4.1 Boundary loading (pressure and tractions).

Following Johnson (1985), the subsurface stresses are given by the following equations:

$$\sigma_{xx} = \frac{2 \cdot \nu \cdot G}{1 - 2 \cdot \nu} \cdot \left(\frac{\partial u_x}{\partial x} + \frac{\partial u_y}{\partial y} + \frac{\partial u_z}{\partial z} \right) + 2 \cdot G \cdot \frac{\partial u_x}{\partial x} \quad (4.1)$$

$$\sigma_{yy} = \frac{2 \cdot \nu \cdot G}{1 - 2 \cdot \nu} \cdot \left(\frac{\partial u_x}{\partial x} + \frac{\partial u_y}{\partial y} + \frac{\partial u_z}{\partial z} \right) + 2 \cdot G \cdot \frac{\partial u_y}{\partial y} \quad (4.2)$$

$$\sigma_{zz} = \frac{2 \cdot \nu \cdot G}{1 - 2 \cdot \nu} \cdot \left(\frac{\partial u_x}{\partial x} + \frac{\partial u_y}{\partial y} + \frac{\partial u_z}{\partial z} \right) + 2 \cdot G \cdot \frac{\partial u_z}{\partial z} \quad (4.3)$$

$$\tau_{xy} = G \cdot \left(\frac{\partial u_x}{\partial y} + \frac{\partial u_y}{\partial x} \right) \quad (4.4)$$

$$\tau_{yz} = G \cdot \left(\frac{\partial u_y}{\partial z} + \frac{\partial u_z}{\partial y} \right) \quad (4.5)$$

$$\tau_{zx} = G \cdot \left(\frac{\partial u_z}{\partial x} + \frac{\partial u_x}{\partial z} \right) \quad (4.6)$$

where G is the shear modulus of elasticity. The displacements are given by the following equations:

$$u_x = \frac{1}{4 \cdot \pi \cdot G} \cdot \left[\begin{array}{l} 2 \cdot \frac{\partial^2 F_1}{\partial z^2} - \frac{\partial^2 H_1}{\partial x \partial z} + 2 \cdot \nu \cdot \left(\frac{\partial^2 F_1}{\partial x^2} + \frac{\partial^2 G_1}{\partial x \partial y} + \frac{\partial^2 H_1}{\partial x \partial z} \right) - \\ z \cdot \left(\frac{\partial^3 F_1}{\partial x^2 \partial z} + \frac{\partial^3 G_1}{\partial x \partial y \partial z} + \frac{\partial^3 H_1}{\partial x \partial z^2} \right) \end{array} \right] \quad (4.7)$$

$$u_y = \frac{1}{4 \cdot \pi \cdot G} \cdot \left[\begin{array}{l} 2 \cdot \frac{\partial^2 G_1}{\partial z^2} - \frac{\partial^2 H_1}{\partial y \partial z} + 2 \cdot \nu \cdot \left(\frac{\partial^2 F_1}{\partial x \partial y} + \frac{\partial^2 G_1}{\partial y^2} + \frac{\partial^2 H_1}{\partial y \partial z} \right) - \\ z \cdot \left(\frac{\partial^3 F_1}{\partial x \partial y \partial z} + \frac{\partial^3 G_1}{\partial y^2 \partial z} + \frac{\partial^3 H_1}{\partial y \partial z^2} \right) \end{array} \right] \quad (4.8)$$

$$u_z = \frac{1}{4 \cdot \pi \cdot G} \cdot \left[\begin{array}{l} \frac{\partial^2 H_1}{\partial z^2} + (1 - 2 \cdot \nu) \cdot \left(\frac{\partial^2 F_1}{\partial x \partial z} + \frac{\partial^2 G_1}{\partial y \partial z} + \frac{\partial^2 H_1}{\partial z^2} \right) - \\ z \cdot \left(\frac{\partial^3 F_1}{\partial x \partial z^2} + \frac{\partial^3 G_1}{\partial y \partial z^2} + \frac{\partial^3 H_1}{\partial z^3} \right) \end{array} \right] \quad (4.9)$$

where

$$F_1 \equiv \iint_A \bar{\tau}_{zx}(\xi, \psi, t) \cdot \Omega \cdot d\xi \cdot d\psi \quad (4.10)$$

$$G_1 \equiv \iint_A \bar{\tau}_{zy}(\xi, \psi, t) \cdot \Omega \cdot d\xi \cdot d\psi \quad (4.11)$$

$$H_1 \equiv \iint_A p(\xi, \eta, t) \cdot \Omega \cdot d\xi \cdot d\psi \quad (4.12)$$

where

$$\Omega \equiv z \cdot \ln \left[z + \sqrt{(x - \xi)^2 + (y - \psi)^2 + z^2} \right] - \sqrt{(x - \xi)^2 + (y - \psi)^2 + z^2} \quad (4.13)$$

The rest of the stress analysis is part of the author's Doctoral thesis (Nikas, 1999, chapter 4) and will not be repeated here. What is done essentially is to apply numerical integration of the surface pressure and tractions over the contact and then calculate the subsurface stresses from equations (4.1)-(4.6).

This is by far the most time-consuming process of the CVT model. The numerical integrations require a large number (thousands) of integration nodes to achieve acceptable accuracy. Using a 266 MHz personal computer, these calculations can easily consume several days of CPU time, even for low grid resolutions. This is particularly problematic in rough (asperity) contacts (as is case in the TOROTRAK IVT), because the number of grid points required must be sufficiently large to account for the stress effect of roughness on the near surface layers, which is of importance in the CVT life calculations.

The previous analysis covers the case of elastic stresses and displacements. However, allowance was made for localised (asperity) plastic deformations, by using the term D_p in equation (3.47). It has already been mentioned (see the last of the boundary conditions in § 3.8) that when the calculated surface pressure at a point exceeds a plasticity limit, then the surface at the close vicinity of the aforementioned point resides to allow a pressure relief, until the pressure is reduced to the level of the plasticity limit. The plastically displaced material is assumed to be accommodated below the surface, without any significant change of the macroscopic dimensions of the solid body. This can be visualised by thinking of a roughness asperity being pressed into the surface, like a nail enters a wooden board. In reality, material around the asperity will be slightly raised to allow for the accommodation of part of the asperity under the surface (like the raised shoulders of a sharp debris dent), but such effects are considered having insignificant influence on the overall stress analysis and, correspondingly, fatigue life calculations, providing that they are localised (isolated events). If the latter is not true, the contact is definitely in a state of gross plastic damage (scuffing), which arguably cancels the necessity for any further stress analysis.

5. Fatigue life equation

The fatigue life model used extensively in the literature is the Ioannides-Harris (1985) model, which is an extension of the original (1947) Lundberg-Palmgren (L-P) model. The Ioannides-Harris (I-H) model uses an endurance limit, below which fatigue will not occur. Any subsurface stresses that are greater (in absolute value) than the endurance limit, do not contribute to the risk of fatigue. Additionally, the I-H model spreads the fatigue life calculations to elemental volumes of material, whereas the L-P model considers the studied body as one entity. The I-H model reads as follows:

$$\ln\left(\frac{1}{S}\right) \cong A \cdot N^{e'} \cdot \int_{V_R} \frac{(|\sigma| - \sigma_u)^c}{z'^{h'}} \cdot dV \quad (5.1)$$

where S is the probability of survival ($0 < S < 1$) after N millions of stress cycles, A is an experimentally derived proportionality constant, e' is the life exponent constant (Weibull slope, usually $e' = 1.1-1.5$), σ stands for subsurface stress (in N/mm^2 or MPa), σ_u is the endurance limit (in N/mm^2 or MPa, $\sigma_u \geq 0$), z' is a stress-weighted average depth (in mm), c is the stress criterion exponent (for bearings $c = 31/3$), h' is the depth exponent (typical $h' = 2.3$), and V_R is the risk volume of material where $|\sigma| > \sigma_u$ (in mm^3).

The proportionality constant A can be calculated if one experimental point (σ_0 , L_{xx}) is known, where L_{xx} is the fatigue life that xx % (e.g. 10 %) of a batch of components will endure (i.e., xx % of components will endure L_{xx} millions of stress cycles, when σ in the integral of equation (5.1) is set equal to σ_0). Moreover, Lubrecht *et al.* (1990) argue that the depth exponent h' can be set equal to zero, especially in rough/asperity contacts, thus eliminating the term of the average depth z' from the fatigue life equation (5.1). This route is followed in the current CVT model.

Therefore:

$$\ln\left(\frac{1}{S}\right) \cong A \cdot N^{e'} \cdot \int_{V_R} (|\sigma| - \sigma_u)^c \cdot dV \quad (\text{setting } h' = 0 \text{ in equation (5.1)}) \quad (5.2)$$

What is usually of importance in these calculations is the L_{10} ($S = 0.9$) or L_{50} ($S = 0.5$) life.

Rearranging equation (5.2), the fatigue life and the probability of survival are given by the following equations:

$$N \cong \left[\frac{\ln\left(\frac{1}{S}\right)}{A \cdot \int_{V_R} (|\sigma| - \sigma_u)^c \cdot dV} \right]^{1/e'} \quad (5.3)$$

$$S \cong \exp \left[-A \cdot N^{e'} \cdot \int_{V_R} (|\sigma| - \sigma_u)^c \cdot dV \right] \quad (5.4)$$

There is a number of fatigue-stress criteria used in the literature, but two of them are the most widely used: the Deformation Energy (von Mises) criterion and the Maximum Shear Stress criterion. Both of these two criteria are used in the CVT model.

5.1 Deformation Energy (von Mises) fatigue-stress criterion

According to this criterion, the equivalent stress σ to be used in the fatigue life equation is given as

$$\sigma = \sqrt{\frac{(\sigma_{xx} - \sigma_{yy})^2 + (\sigma_{yy} - \sigma_{zz})^2 + (\sigma_{zz} - \sigma_{xx})^2 + 6 \cdot (\tau_{xy}^2 + \tau_{yz}^2 + \tau_{zx}^2)}{2}} \quad (5.5)$$

This criterion is simple and uses all six components of the stress tensor to calculate the equivalent stress.

5.2 Maximum Shear Stress criterion

According to this criterion, the equivalent stress σ to be used in the fatigue life equation is the maximum shear stress, corrected by the hydrostatic stress. Before giving the equation, which defines the equivalent stress σ , some auxiliary variables must be defined first.

The three stress invariants are:

$$\left. \begin{aligned} J_1 &\equiv \sigma_{xx} + \sigma_{yy} + \sigma_{zz} \\ J_2 &\equiv \sigma_{xx} \cdot \sigma_{yy} + \sigma_{yy} \cdot \sigma_{zz} + \sigma_{zz} \cdot \sigma_{xx} \\ J_3 &\equiv \sigma_{xx} \cdot \sigma_{yy} \cdot \sigma_{zz} + 2 \cdot \tau_{xy} \cdot \tau_{yz} \cdot \tau_{zx} - \sigma_{xx} \cdot \tau_{yz}^2 - \sigma_{yy} \cdot \tau_{zx}^2 - \sigma_{zz} \cdot \tau_{xy}^2 \end{aligned} \right\} \quad (5.6)$$

The following auxiliary variables C_1 , C_2 and C_3 are now defined:

$$C_1 \equiv \frac{J_1^2}{3} - J_2, \quad C_2 \equiv J_3 - \frac{J_1 \cdot J_2}{3} + \frac{2 \cdot J_1^3}{27} \quad (5.7)$$

$$C_3 \equiv \arccos\left(\frac{C_2}{2 \cdot C_1^{3/2}}\right) \quad (5.8)$$

The three principal stresses σ_1 , σ_2 , σ_3 are calculated as follows:

$$\left. \begin{aligned} \sigma_1 &= \frac{J_1}{3} + 2 \cdot \sqrt{C_1} \cdot \cos\left(\frac{C_3}{3}\right) \\ \sigma_2 &= \frac{J_1}{3} + 2 \cdot \sqrt{C_1} \cdot \cos\left(\frac{C_3 + 2 \cdot \pi}{3}\right) \\ \sigma_3 &= \frac{J_1}{3} + 2 \cdot \sqrt{C_1} \cdot \cos\left(\frac{C_3 + 4 \cdot \pi}{3}\right) \end{aligned} \right\} \quad (5.9)$$

The equivalent stress σ can now be calculated as follows:

$$\sigma = \tau_{\max} - 0.3 \cdot p_H = \frac{\max\{\sigma_1, \sigma_2, \sigma_3\} - \min\{\sigma_1, \sigma_2, \sigma_3\}}{2} - 0.3 \cdot \frac{J_1}{3} \quad (5.10)$$

where τ_{\max} is the maximum shear stress (equal to the difference of the maximum and the minimum principal stress, divided by 2) and p_H is the hydrostatic pressure ($p_H = J_1/3$).

Moreover, the endurance limit σ_u in this criterion is defined as follows:

$$\sigma_u = \left\{ \begin{array}{l} 266 \text{ MPa if } |\tau_{\max} + 0.3 \cdot p_H| \leq 600 \text{ MPa} \\ 798 - 0.88667 \cdot |\tau_{\max} + 0.3 \cdot p_H| \text{ if } 600 \text{ Mpa} < |\tau_{\max} + 0.3 \cdot p_H| \leq 900 \text{ MPa} \\ 0 \text{ if } |\tau_{\max} + 0.3 \cdot p_H| > 900 \text{ MPa} \end{array} \right\} \quad (5.11)$$

6. Contact fatigue – comparison of rolling bearings and CVTs

Rolling bearings' purpose is to offer load support, transferring load between the bearing rings through the bearing rolling elements. The contact between a rolling element and a ring is of the rolling type, with very limited amounts of sliding (hence the name *rolling* bearings). CVTs on the other side, essentially transmit power between two disks and usually work with substantial amounts of sliding. When it comes to fatigue life calculations, there are some basic differences between rolling bearings and CVTs. Here follows a list of some important differences.

- (a) A rolling bearing contact is mainly under normal pressure. A CVT contact is mainly under a combination of normal pressure and traction (shear). The normal pressure in rolling bearings can be quite higher than in CVTs (e.g. 4-5 GPa for rolling bearings versus 1-2 GPa for CVTs).
- (b) The surface quality of rolling bearings is usually of very high standards. CVTs have usually worse surface finish (rougher contact surface).
- (c) As a result of (b), CVTs often work at very low λ -ratio (the ratio of the minimum film thickness to the composite RMS surface roughness), with a large amount of asperity interactions, when this kind of interaction is very limited in high quality rolling bearings.
- (d) As a result of (c), CVT contacts often exhibit a large proportion of local asperity plastic deformations. As a matter of fact, the roughness asperities often carry a significant portion of the supported load, when in rolling bearings, it is the lubricant film that supports almost all of the load.
- (e) Following (c) and (d) (roughness asperity interactions in CVTs), the stressing of a typical CVT contact exhibits a lot of solid shearing, besides the usual fluid internal shearing. Friction among colliding asperities brings the high-risk subsurface shear stress zone closer to the surface, which can be realised if the contact between two asperities is visualised as a micro-Hertzian contact. Moreover, asperity collisions result in local frictional heating and, hence, the development of thermal stresses. As is explained in § 2.2, thermal stresses originating from surface frictional heating have their highest strength on the very top layers below the surface. Such transient and localised thermal stress fields below colliding asperities are combined with the elastoplastic normal and, especially, shear stress fields. The result is a zone of high risk of fatigue very close

to the surface. In contrast, the high-risk stress zone in rolling bearing contacts lies much deeper below the surface, as is normally predicted by the Hertzian theory of elastic contact.

- (f) Contact fatigue is normally associated with spalling, i.e. when a piece of material breaks away from the surface. Spalling is divided into two phases: crack initiation and crack propagation. In rolling bearings of high quality surface finish, the phase of crack initiation is far longer than the phase of crack propagation. This observation is indeed addressed in the development of the Ioannides-Harris (1985) fatigue life model. Once initiated, a crack usually propagates rapidly in rolling bearings because of the high level of loading that bearings tolerate. This macro-spall formation is characteristic of the classical rolling contact fatigue. In the case of CVTs (traction drives) however, the high levels of traction and often asperity thermoelastoplastic interaction events can result in a different form of contact fatigue, which is surface initiated. Instead of distinctive macro-spalling, it is common to observe micro-pitting, which, when viewed with naked eye, has a grey/matt appearance. This form of fatigue has not been clearly understood, but it can be speculated that a possible explanation lies in the asperity-interaction hypothesis. Following a previous work (Nikas, 1999), the author believes that asperity flash temperatures (which are often calculated to be very high, e.g. over 1000 °C) can play a significant role in the initiation of thermo-cracks, which, as explained earlier, originate from the surface. Once initiated, these fine surface cracks can propagate rapidly, especially in lubricated contacts where it is widely speculated that the highly pressurised lubricant enters the cracks and opens them up by means of its hydraulic pressure.
- (g) As is explained in (f), contact fatigue in rolling bearings is normally initiated at the deep subsurface shear stress zone, as predicted by the classical Hertzian theory. The cracks then reach the surface and result in spalling. In CVTs, contact fatigue normally initiates from the surface. Fine micro-cracks propagate downwards, until they meet the deep subsurface shear stress zone. In their journey, CVT contact micro-cracks have to pass through a relatively stress-free zone, named quiescent zone, before they reach the deep subsurface shear stress zone. If there are steel inclusions in this quiescent zone, they may act as stress raisers, assisting in the propagation of the surface micro-cracks. The cleanliness of

steel will, therefore, play a role in the contact fatigue life. This is not an issue with modern rolling bearings, where the steel used is usually of the highest quality (without inclusions). For CVTs however, steel cleanliness may be more of an issue and must be given attention if long fatigue lives are to be achieved.

- (h) As is explained in § 2.1, lubricant thermal effects play an important role in the lubrication and traction capacity of CVTs. Because of the high shearing of the lubricant in typical CVT contacts, the lubricant is internally heated to such an extent that its dynamic viscosity is reduced. This reduction counteracts the viscosity increase that follows the substantial compression of the lubricant in the high-pressure central zone of a contact. Typical lubricant temperature increase due to (mainly) shearing in a sliding contact is between 50-100 °C. If such a temperature increase is combined with the normal operation (bulk) temperature of the lubricant (which, in the case of TOROTRAK's IVT could be more than 100 °C), the overall local lubricant temperature could easily exceed 150-200 °C. This is above the lubricant-film strength (desorption or melting point), even when lubricants with special EP additives are used (maximum strength of about 150 °C). As a result, the lubricant in a CVT contact may experience local melting and lose its protective power. This is not an issue in rolling bearings, which operate with very limited sliding and, hence, do not experience substantial lubricant frictional heating.
- (i) A rolling bearing usually operates under less transient conditions than a CVT. For example, the rapid accelerations and changes of the transmitted power are quite common in CVT contacts, whereas these events are more rare in rolling bearings. It is explained in § 2.5 that such transient phenomena can have detrimental effects on the lubrication (film thinning or collapse) and, consequently, the fatigue life of the cooperating components. In rolling bearings this is known as “smearing”.

7. Examples

Several example cases are analysed in this section in order to show the application of the developed model and accompanying computer program. The differences among the various cases are chosen in a way to show the effect of important parameters, as are the contact load, sliding speed and surface roughness, on the lubrication, stressing and fatigue life of the contact.

Two surface roughness textures were used in the examples. The first represents a real example and was measured by a Talysurf device in TOROTRAK. The measurements were performed on the surface of a roller and figure 7.1 shows a flattened portion of the surface, with dimensions $8 \text{ mm} \times 4 \text{ mm}$.

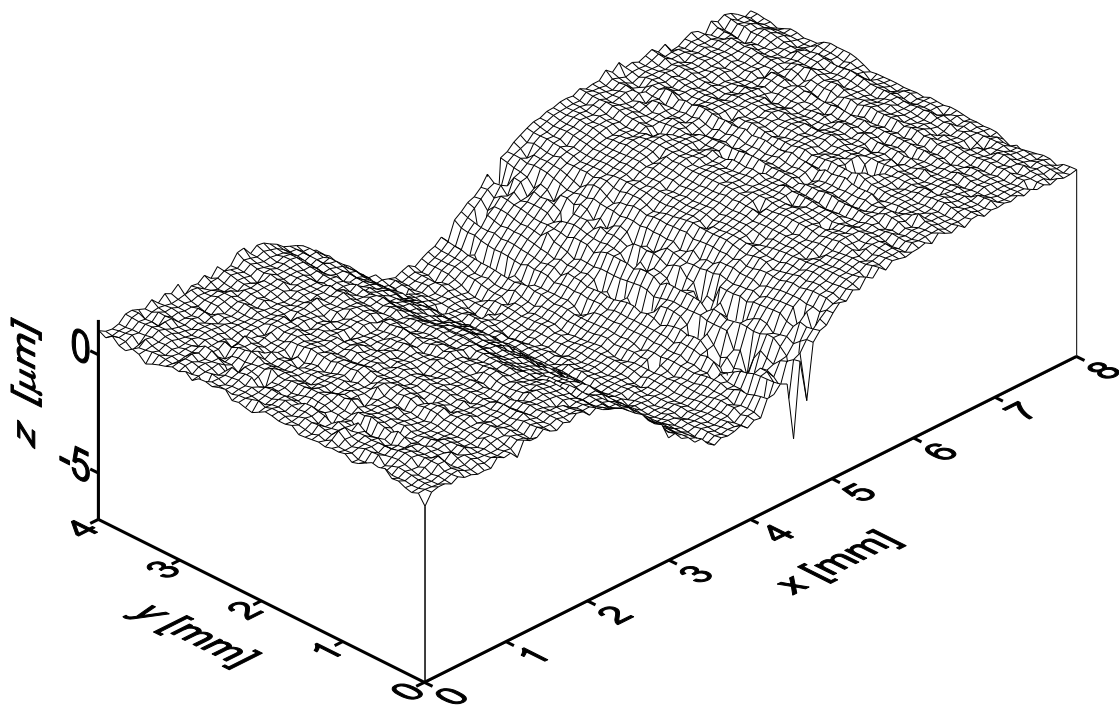


Figure 7.1 Portion of the roller's working surface ($\text{RMS} \cong 1.45 \text{ } \mu\text{m}$, $R_{\text{max}} \cong 13.2 \text{ } \mu\text{m}$).

For the surface shown in figure 7.1, $\text{RMS} \cong 1.45 \text{ } \mu\text{m}$. Also, the maximum asperity height is $3.5 \text{ } \mu\text{m}$ and the maximum valley depth is $9.7 \text{ } \mu\text{m}$. The RMS value is quite

high because the large valley shown in the figure is taken into account. If the valley is ignored, the RMS roughness value would be around 0.2-0.3 μm .

Due to lack of roughness data for the cooperating surface of the toroidal disk, an artificially created, random roughness was assumed, with an RMS value of 0.26 μm (according to TOROTRAK, the RMS range for the roller and disk is 0.13-0.23 μm). The peak asperity of that artificial surface and the deepest valley have the same height, namely 0.45 μm . Figure 7.2 shows a portion of the artificially created disk surface.

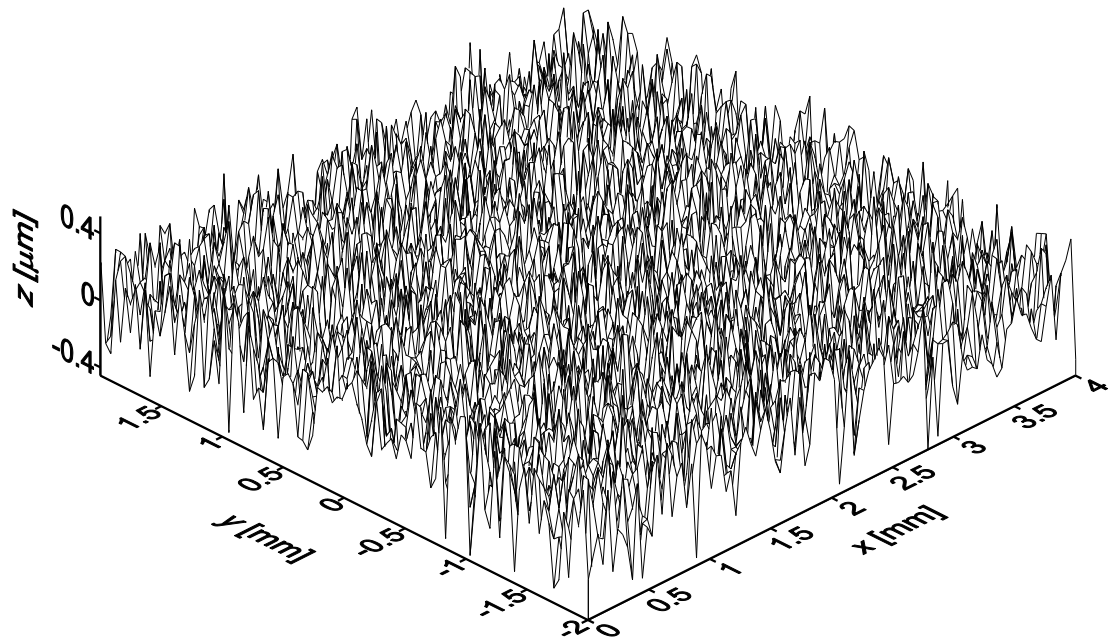


Figure 7.2 Artificially created random surface (RMS \cong 0.26 μm , $R_{\text{max}} \cong$ 0.9 μm).

Table 7.1 lists the data that are common for all examples and figure 7.3 shows the main components of the variator and their basic dimensions.

Table 7.1

Data used in all examples	
Lubricant (traction fluid)	Santotrac 50
“Height” of the variator, H (see figure 7.3)	55 mm
“Radius” of the variator, r (see figure 7.3)	50 mm
Radius of curvature of the roller, $r_x^{(\text{roller})}$	50 mm
Radius of curvature of the roller, $r_y^{(\text{roller})}$	30 mm
Working angle, φ (see figure 7.3)	10° (close to maximum torque)
Moduli of elasticity, $E_{\text{roller}}, E_{\text{disk}}$	207 GPa
Poisson ratios, $\nu_{\text{roller}}, \nu_{\text{disk}}$	0.3
Density-pressure-temperature equation (3.36) constants, c_1, c_2, c_3	$c_1 = 6 \cdot 10^{-10} \text{ Pa}^{-1}$, $c_2 = 17 \cdot 10^{-10} \text{ Pa}^{-1}$, $c_3 = 65 \cdot 10^{-5} \text{ }^\circ\text{C}^{-1}$
Ambient density of the lubricant, ρ_0	870 kg/m ³ (estimation)
Viscosity-pressure-temperature equation used	Barus (equation (3.23))
Lubricant limiting-shear-stress equation (3.35) constants, τ_0, γ, δ	$\tau_0 = 317 \cdot 10^5 \text{ Pa}$, $\gamma = 0.093$, $\delta = 317000 \text{ Pa}/^\circ\text{C}$
Tangential speed of the roller in y axis, v_{roller}	zero
Tangential speed of the toroidal disk in y axis, v_{disk}	zero
Rheological model used	Bair-Winer (see § 3.2.2)

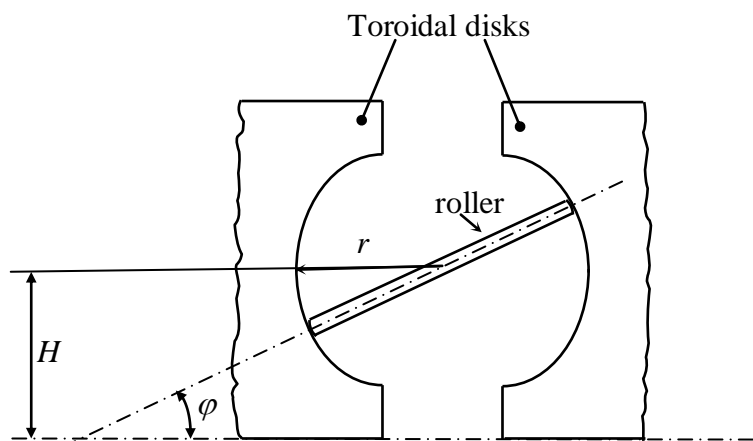


Figure 7.3 Basic dimensions of the variator.

The effective radii of curvature R_x and R_y (see equations (3.37)) can be calculated from the data given in table 7.1, namely the radii of curvature of the roller, the working angle φ , the radius of the variator r , and the height of the variator H :

$$R_x = r \cdot \left[1 - \frac{r}{H} \cdot \sin(\varphi) \right] , \quad R_y = \frac{r \cdot r_y^{(\text{roller})}}{r - r_y^{(\text{roller})}} \quad (7.1)$$

Changes of the working angle φ during the operation of the variator result in changes of R_x according to equations (7.1) and this is taken into account in the solution of the (transient) lubrication equation developed for this model (equation (3.20)).

The radii of curvature of the toroidal disks are given by

$$r_x^{(\text{disk})} = -\frac{H + r \cdot \sin(\varphi)}{\sin(\varphi)} , \quad r_y^{(\text{disk})} = -r \quad (7.2)$$

Based on the data given in table 7.1, the radii of curvature of the toroidal disks are

$$r_x^{(\text{disk})} \cong -367 \text{ mm} \quad \text{and} \quad r_y^{(\text{disk})} \cong -50 \text{ mm} .$$

Table 7.2 shows a parametric study for test-cases similar to those encountered in a TOROTRAK IVT, covering low and high loads, low and higher operating oil temperatures, and low and higher sliding conditions. These cases represent examples where there is no roughness-asperity interaction (according to the calculated results). All results have been obtained from the computer program created for this project.

The results of table 7.2 were obtained using a grid of 100×100 nodes covering an area $-1.6 \cdot D_x \leq x \leq 1.6 \cdot D_x$ and $-1.6 \cdot D_y \leq y \leq 1.6 \cdot D_y$ (this is the same as choosing the 50×50 resolution for the EHL solution in the computer program). This resolution is not sufficient for an accurate addressing of rough surfaces but helps obtain results quickly. Therefore, the results of table 7.2 must be interpreted in relation to each other rather than as absolute figures.

Table 7.2

Parametric study – Cases with no roughness asperity interactions					
Randomly rough surfaces (figure 7.2).					
EHL grids: 100×100 (denoted 50×50 in the computer program),					
covering $-1.6 \cdot D_x \leq x \leq 1.6 \cdot D_x$ and $-1.6 \cdot D_y \leq y \leq 1.6 \cdot D_y$					
Data (see also table 7.1) $P, \theta_0, (u_{\text{roller}}, u_{\text{disk}})$	h_{min} [μm]	λ	μ_{roller}	μ_{disk}	p_0 [GPa]
3 kN, 60 °C, (10, 8) m/s	1.02	2.8	0.082	0.079	1.35
3 kN, 60 °C, (10, 9.7) m/s	0.80	2.2	0.082	0.079	1.35
3 kN, 80 °C, (10, 8) m/s	0.70	1.9	0.077	0.075	1.35
3 kN, 80 °C, (10, 9.7) m/s	0.76	2.1	0.077	0.074	1.35
3 kN, 100 °C, (10, 8) m/s	0.71	1.9	0.074	0.070	1.35
3 kN, 100 °C, (10, 9.7) m/s	0.70	1.9	0.073	0.069	1.35
6 kN, 60 °C, (10, 8) m/s	1.55	4.2	0.078	0.074	1.70
6 kN, 60 °C, (10, 9.7) m/s	1.64	4.5	0.077	0.074	1.70
6 kN, 80 °C, (10, 8) m/s	1.53	4.2	0.082	0.079	1.70
6 kN, 80 °C, (10, 9.7) m/s	1.32	3.6	0.081	0.077	1.70
6 kN, 100 °C, (10, 8) m/s	0.86	2.3	0.080	0.076	1.70
6 kN, 100 °C, (10, 9.7) m/s	1.12	3.0	0.080	0.074	1.70
10 kN, 60 °C, (10, 8) m/s	1.57	4.3	0.085	0.083	2.01
10 kN, 60 °C, (10, 9.7) m/s	3.42	9.3	0.082	0.079	2.01
10 kN, 80 °C, (10, 8) m/s	1.10	3.0	0.082	0.079	2.01
10 kN, 80 °C, (10, 9.7) m/s	1.64	4.5	0.079	0.075	2.01
10 kN, 100 °C, (10, 8) m/s	0.15	0.4	0.080	0.077	2.01
10 kN, 100 °C, (10, 9.7) m/s	0.43	1.2	0.080	0.077	2.01
20 kN, 100 °C, (10, 8) m/s *	2.62	7.1	0.086	0.083	2.54

* Some roughness asperities for this case were plastically deformed, which explains the increased film thickness.

By studying the figures of table 7.2, the following conclusions are drawn.

1. The effect of load on the minimum film thickness is not clear because of the flattening of individual asperities, which could even be plastically deformed (see last case) by the fluid pressure. Increased load could result in thicker minimum film thickness.
2. The minimum film thickness for almost all cases is sufficient to allow for unproblematic operation. This is also reflected on the calculated lambda ratios. However, these results are for steady-state operation. Transient events like a load or speed change could cause film thinning.
3. The operating temperature of the lubricant affects the results rather significantly. Increased temperatures result in thinner films and this is clear by comparing the results for 60 °C, 80 °C and 100 °C. This effect is of course very well known and it is important to see it quantified in a realistic study. The conclusion is that high temperatures must be avoided by cooling the lubricant to an acceptable level (for example, down to 60 °C).
4. The operating temperature also affects the effective traction coefficients. Higher temperatures result in slightly lower traction coefficients, which, when ignoring lubricant thermal effects, is a consequence of the limiting shear stress of the lubricant being reached for lower pressure (see equation (3.35)).
5. Local thermal effects have been ignored; if accounted for, the minimum film thickness is expected to be reduced. This may result in asperities coming into solid contact.
6. The calculated traction coefficients are in the range experimentally found for such cases. The inclusion of lubricant thermal effects in the model would reduce the effective traction coefficients but, generally, the calculated traction is considered realistic.
7. The results are related to the specific roughness texture used (figure 7.2). This will be made clear when studying the results shown in table 7.3, which refer to different roughness textures.

In order to make the results more related to a real TOROTRAK IVT example, table 7.3 presents cases where the roller's working surface is that shown in figure 7.1 (real TOROTRAK example). The disk's working surface is again that shown in figure

7.2, i.e. randomly created roughness with parameters (RMS, R_{\max} etc) similar to those normally found in a TOROTRAK IVT.

Table 7.3

Parametric study – Most cases with roughness asperity interactions						
Roller surface as in figure 7.1 (real case), disk surface as in figure 7.2 (artificial).						
EHL grids: 100×100 (denoted 50×50 in the computer program),						
covering $-1.6 \cdot D_x \leq x \leq 1.6 \cdot D_x$ and $-1.6 \cdot D_y \leq y \leq 1.6 \cdot D_y$						
Data (see also table 7.1) $P, \theta_0, (u_{\text{roller}}, u_{\text{disk}})$	h_{\min} [μm]	λ	μ_{roller}	μ_{disk}	p_0 [GPa]	P_s/P [%]
3 kN, 60 °C, (10, 8) m/s	0	0	0.062	0.062	1.35	81
3 kN, 60 °C, (10, 9.7) m/s	0	0	0.073	0.072	1.35	11
3 kN, 80 °C, (10, 8) m/s	0	0	0.053	0.053	1.35	24
3 kN, 80 °C, (10, 9.7) m/s	0	0	0.073	0.072	1.35	1
3 kN, 100 °C, (10, 8) m/s	0	0	0.038	0.038	1.35	1
3 kN, 100 °C, (10, 9.7) m/s	0	0	0.049	0.049	1.35	42
6 kN, 60 °C, (10, 8) m/s	0	0	0.083	0.082	1.70	2
6 kN, 60 °C, (10, 9.7) m/s	0	0	0.087	0.085	1.70	2
6 kN, 80 °C, (10, 8) m/s	0.66	0.4	0.062	0.061	1.70	0
6 kN, 80 °C, (10, 9.7) m/s	0.25	0.2	0.066	0.066	1.70	0
6 kN, 100 °C, (10, 8) m/s	0	0	0.057	0.056	1.70	11
6 kN, 100 °C, (10, 9.7) m/s	0	0	0.075	0.075	1.70	7
10 kN, 60 °C, (10, 8) m/s	0	0	0.091	0.089	2.01	5
10 kN, 60 °C, (10, 9.7) m/s	0	0	0.091	0.089	2.01	4
10 kN, 80 °C, (10, 8) m/s	0	0	0.086	0.084	2.01	7
10 kN, 80 °C, (10, 9.7) m/s	0	0	0.086	0.084	2.01	7
10 kN, 100 °C, (10, 8) m/s	0	0	0.081	0.080	2.01	8
10 kN, 100 °C, (10, 9.7) m/s	0	0	0.081	0.080	2.01	8
20 kN, 100 °C, (10, 8) m/s *	0	0	0.085	0.084	2.54	2

The last column in table 7.3 shows the load supported by solid contact (P_s) as a percentage of the total supported load (P). Using the results presented in table 7.3, the following conclusions are drawn.

1. Roughness asperities can carry a significant proportion of the transmitted load.
2. The traction during asperity interactions can be much less than the traction anticipated when the surfaces are considered smooth. The level of traction during solid contact depends on the friction coefficient for boundary lubrication, which can be lower than the effective traction coefficient during extensive squeeze (without collapse) of lubricant films. If there is a large number of asperities in contact, the overall traction coefficient is ruled by the boundary-lubrication friction coefficient. From this perspective, the accurate estimation of the boundary friction coefficient is vital in the derivation of accurate traction results. Moreover, there may be large areas of solid contact that don't carry a substantial load (because the load is concentrated in other areas) and, hence, areas that don't contribute to the overall traction in the contact. The latter causes a reduction of the calculated overall traction coefficient.
3. In cases of asperity interactions, any traction results will have a degree of inaccuracy if thermoelastic expansion of colliding and frictionally heated asperities is ignored. Such events need to be accounted for if more accurate predictions are of importance.
4. The operating temperature of the lubricant affects the traction coefficients sometimes substantially. The traction is reduced when the lubricant temperature is increased.
5. It is not recommended to compare the results of table 7.3 with each other (compare the different cases) or with those of table 7.2, because each case refers to a different portion of the surfaces and, hence, different roughness profiles. The area of study on a surface is chosen randomly by the computer program.

7.1 An example with extensive asperity interactions

A specific example is presented next, in order to show the pressure, film thickness and shear stress (traction) distributions in a rough contact. This example is the first test case presented in table 7.3 ($P = 3 \text{ kN}$, $\theta_0 = 60 \text{ }^\circ\text{C}$, $u_{\text{roller}} = 10 \text{ m/s}$, $u_{\text{disk}} = 8 \text{ m/s}$). For this case there is substantial asperity interaction, with 81 % of the transmitted load being supported through solid contact. The maximum Hertzian pressure is 1.35 GPa. Figure 7.4 shows the calculated pressure distribution in the contact.

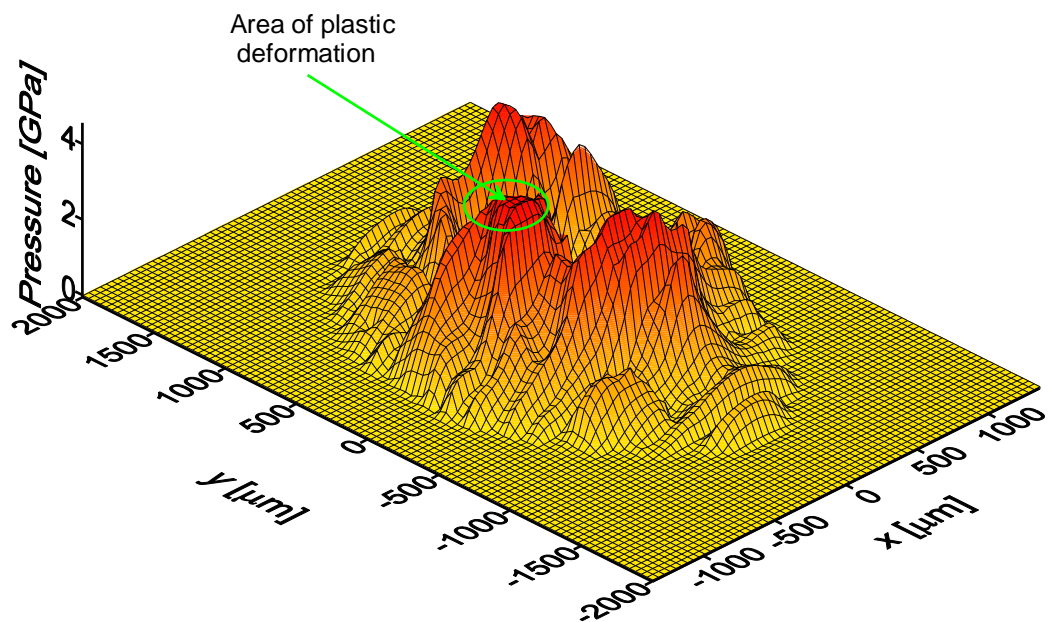


Figure 7.4 Pressure distribution for the first case in table 7.3.

According to figure 7.4, there is an area of plastic deformation at an area of solid contact. The pressure distribution is irregular because of the surface roughness and there are areas of very high pressure that carry most of the load.

Figure 7.5 shows a contour map of the film thickness in the contact. Red areas indicate solid contact and it is obvious that there is extensive asperity interaction that creates isolated patches of intimate asperities.

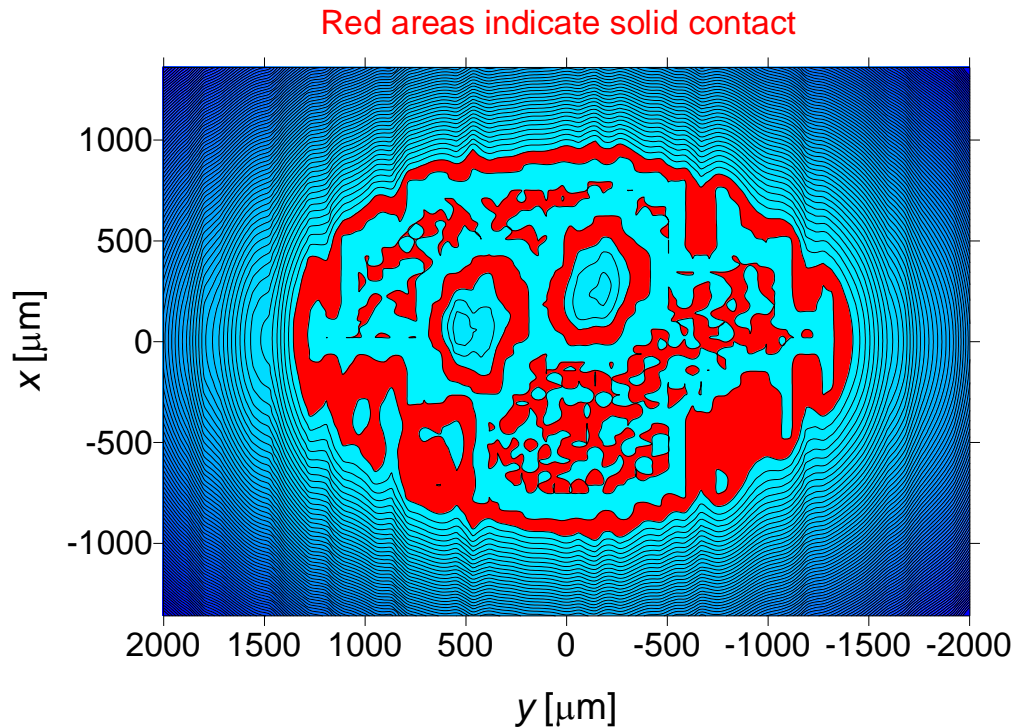


Figure 7.5 Contour map of the film thickness for the first case in table 7.3.

Next, figures 7.6 and 7.7 show maps of the traction (surface shear stress) in the contact. These maps reveal the distribution of traction and the areas that transmit most of the torque between the roller and the toroidal disk. The latter areas are not necessarily regions of solid contact but also areas of high lubricant pressure that approach or reach the limiting shear stress of the traction fluid. It must be noted that due to the redistribution of the shear stress vector in areas where the limiting shear strength of the lubricant has been reached in the direction of sliding (see § 3.4), there is a (very) limited amount of traction along the y -axis, where there is no sliding or rolling and where, normally, there wouldn't be expected any lateral force. However, this is usually very small to be detected (maximum shear stress of about 6 MPa but in opposite directions for $y < 0$ and $y > 0$, which gives a near-zero resultant shear stress along the y -axis).

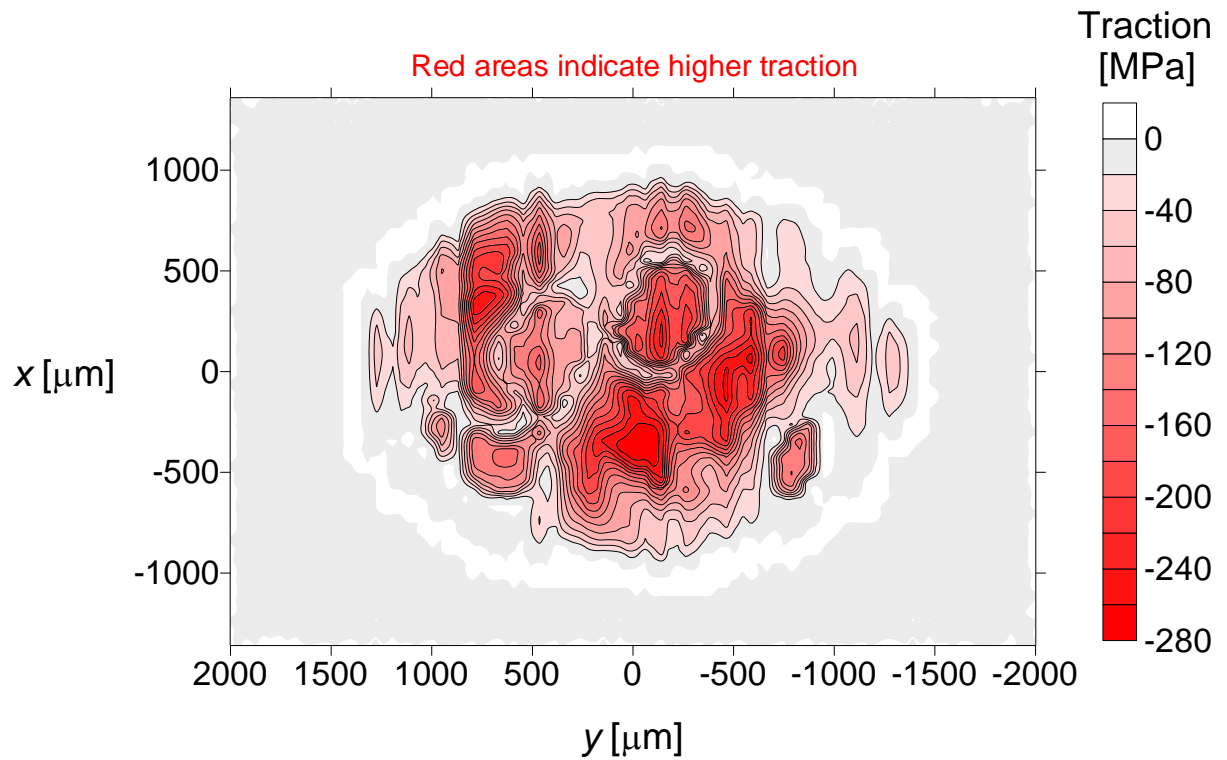


Figure 7.6 Traction (shear stress) on the roller along the axis of sliding (x).

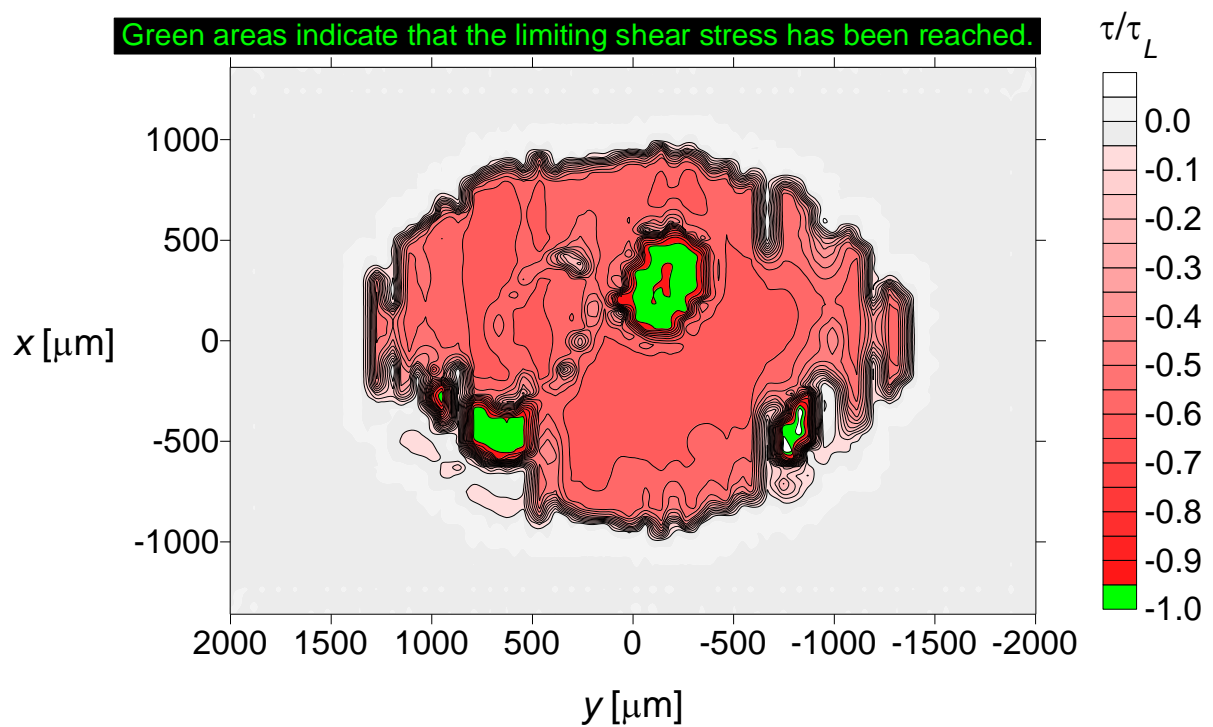


Figure 7.7 Traction over limiting shear stress on the roller along the axis of sliding (x).

Table 7.4 summarises the data and results for the presented example.

Table 7.4

Test case	
Roller surface as in figure 7.1 (real case), disk surface as in figure 7.2 (artificial). Data: $P = 3 \text{ kN}$, $\theta_0 = 60 \text{ }^\circ\text{C}$, $u_{\text{roller}} = 10 \text{ m/s}$, $u_{\text{disk}} = 8 \text{ m/s}$, other data as in table 7.1. EHL grids: 100×100 (denoted 50×50 in the computer program), covering $-1.6 \cdot D_x \leq x \leq 1.6 \cdot D_x$ and $-1.6 \cdot D_y \leq y \leq 1.6 \cdot D_y$	
Length of the contact-ellipse semi-axis x, D_x	850 μm
Length of the contact-ellipse semi-axis y, D_y	1251 μm
Minimum film thickness, h_{min}	0 μm (solid contact)
Lambda ratio, λ	0
Asperity interactions	Yes, extensive.
Maximum Hertzian pressure, p_0	1.35 GPa
Maximum calculated pressure, p	4.44 GPa (local yield)
Average contact pressure, $\frac{P}{\pi \cdot D_x \cdot D_y}$	898 MPa
Effective traction coefficient of the roller, μ_{roller}	0.062
Effective traction coefficient of the toroidal disk, μ_{disk}	0.062
Traction force on the roller on the axis of sliding x, $\mu_{\text{roller}} \cdot P$	186 N
Traction force on the disk on the axis of sliding x, $\mu_{\text{disk}} \cdot P$	186 N
Average traction on the roller on the axis of sliding x, $\frac{\mu_{\text{roller}} \cdot P}{\pi \cdot D_x \cdot D_y}$	56 MPa
Average traction on the toroidal disk on the axis of sliding x, $\frac{\mu_{\text{disk}} \cdot P}{\pi \cdot D_x \cdot D_y}$	56 MPa
Torque on the roller on the axis of sliding x (traction force $\times r$)	$186 \text{ N} \times 0.050 \text{ m} = 9.3 \text{ N}\cdot\text{m}$

7.2 An example of the subsurface stress fields

This section is devoted to the presentation of the subsurface stress fields as they are calculated by the computer program of this project (see also § 4). The test case, a calculated pressure distribution for a rough contact without asperity interactions (and thus full film separation), is shown in figure 7.8.

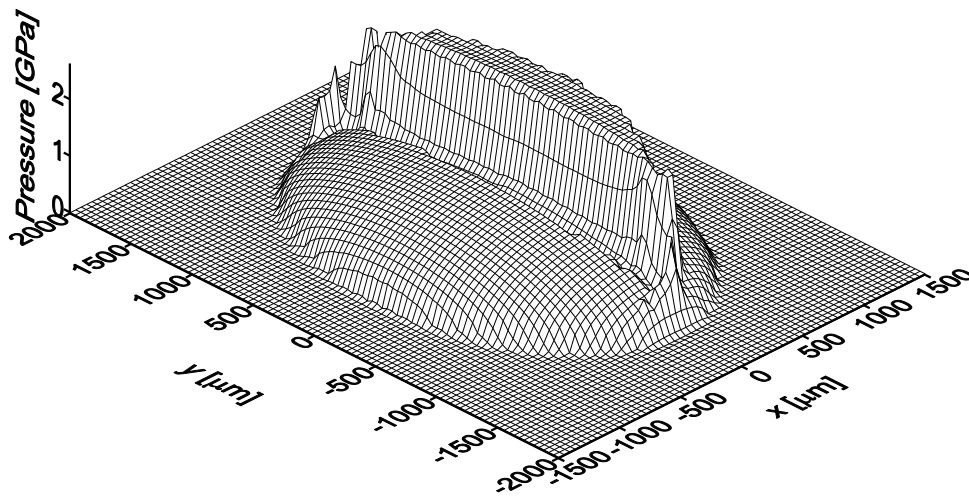


Figure 7.8 Example of pressure distribution ($p_0 = 1.60$ GPa, $p_{\max} = 2.62$ GPa).

The calculated elastohydrodynamic tractions are shown in figures 7.9 and 7.10.

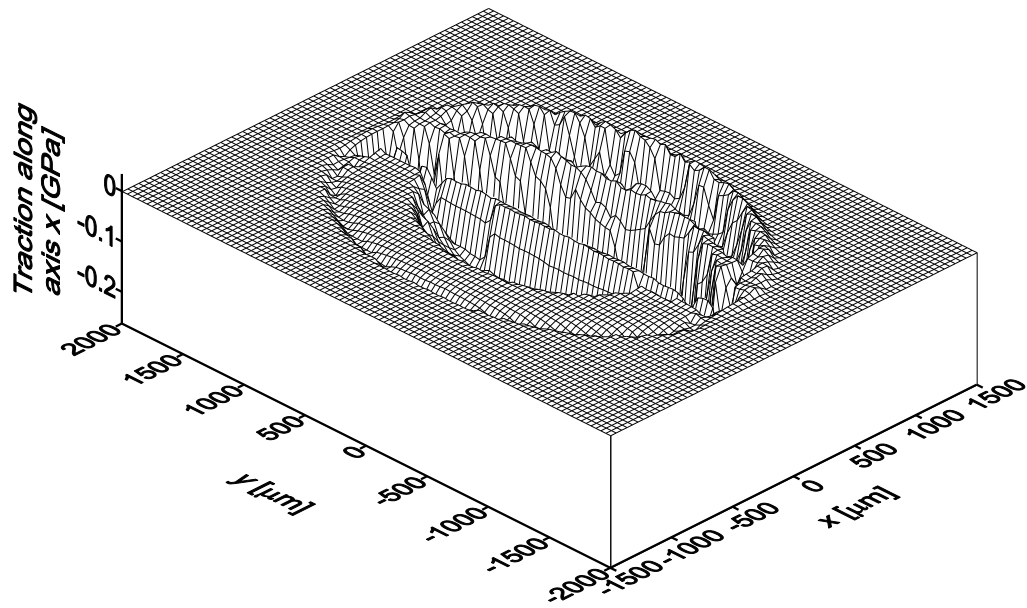


Figure 7.9 Surface traction $\bar{\tau}_{zx}^{(\text{roller})}$.

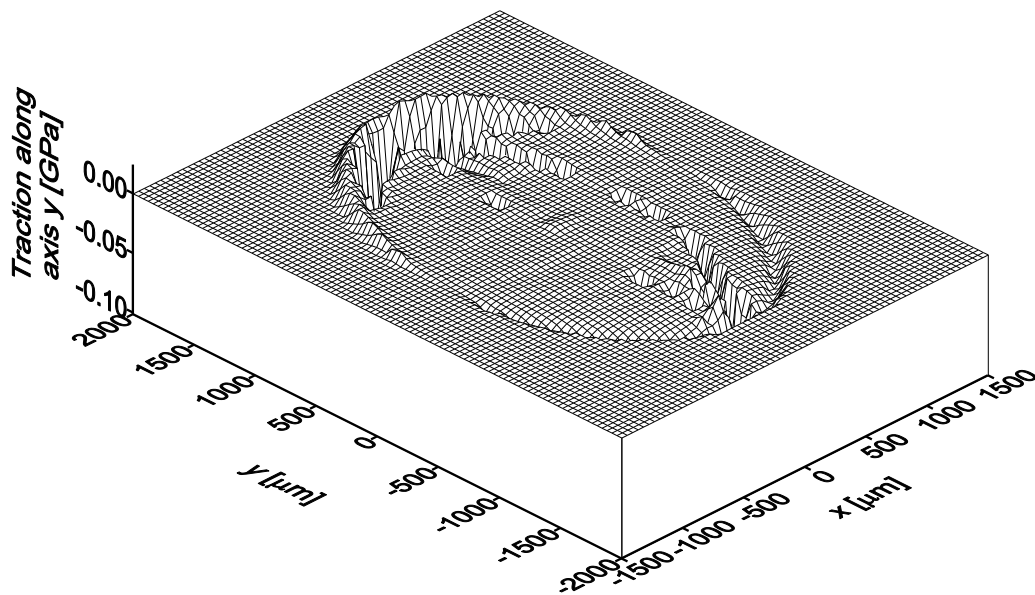


Figure 7.10 Surface traction $\bar{\tau}_{zy}^{(\text{roller})}$.

Following figures 7.8-7.10, figures 7.11-7.16 show the distribution of all six components of the stress tensor, at a depth of 8 μm below the surface.

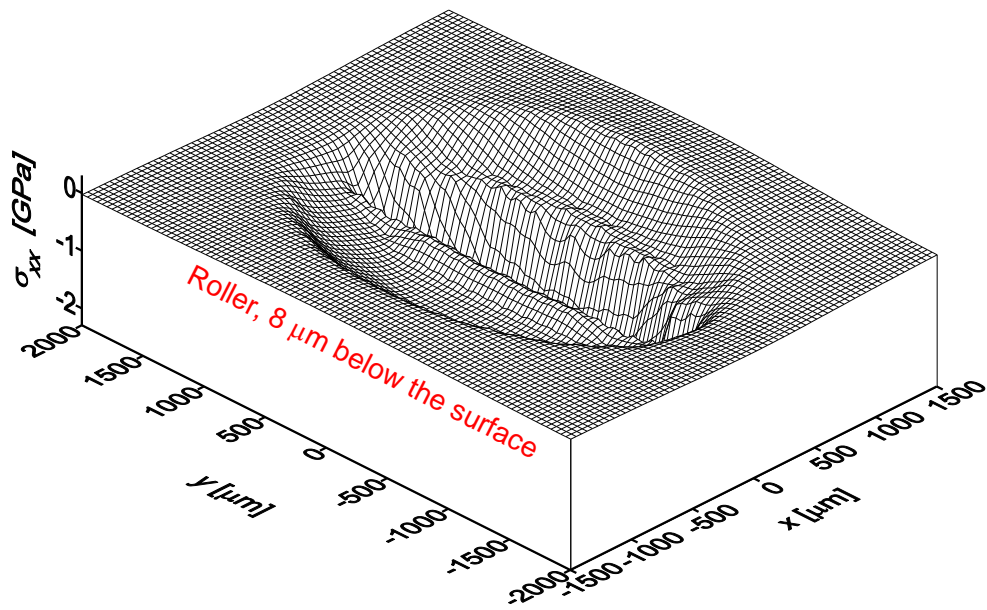


Figure 7.11 Distribution of normal stress σ_{xx} at $z = 8 \mu\text{m}$.

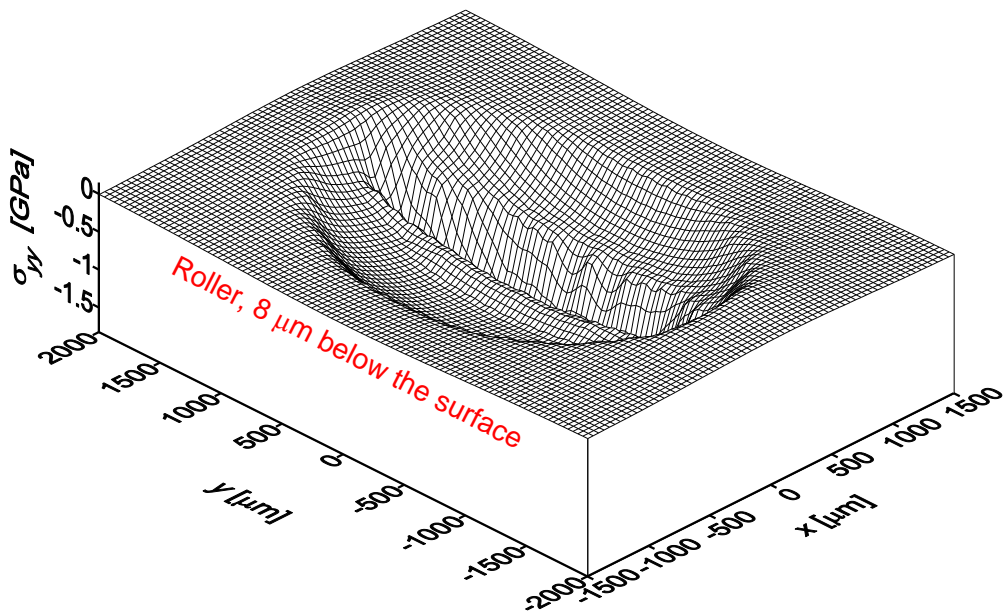


Figure 7.12 Distribution of normal stress σ_{yy} at $z = 8 \mu\text{m}$.

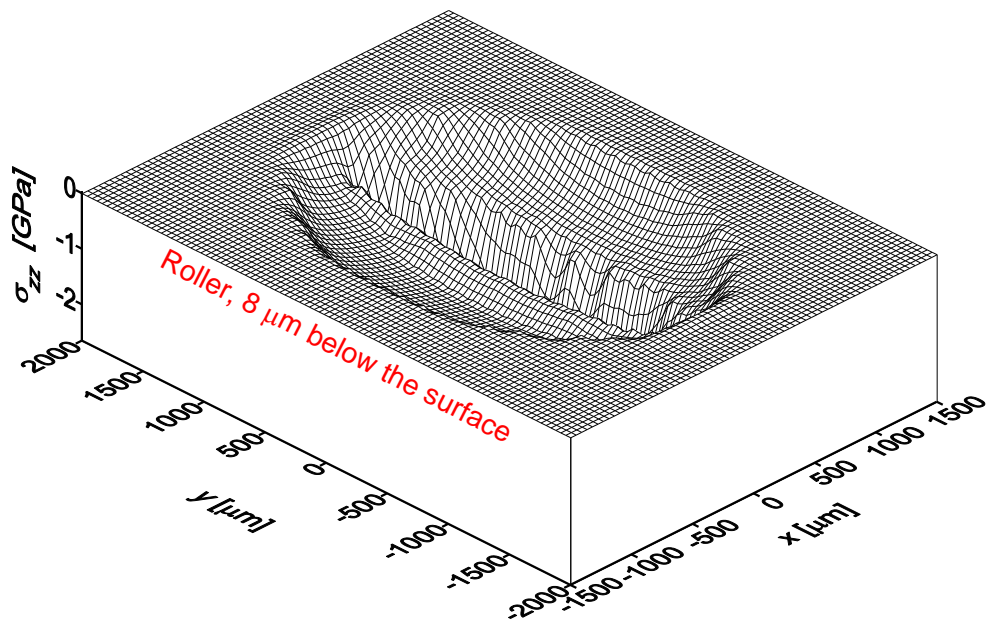


Figure 7.13 Distribution of normal stress σ_{zz} at $z = 8 \mu\text{m}$.

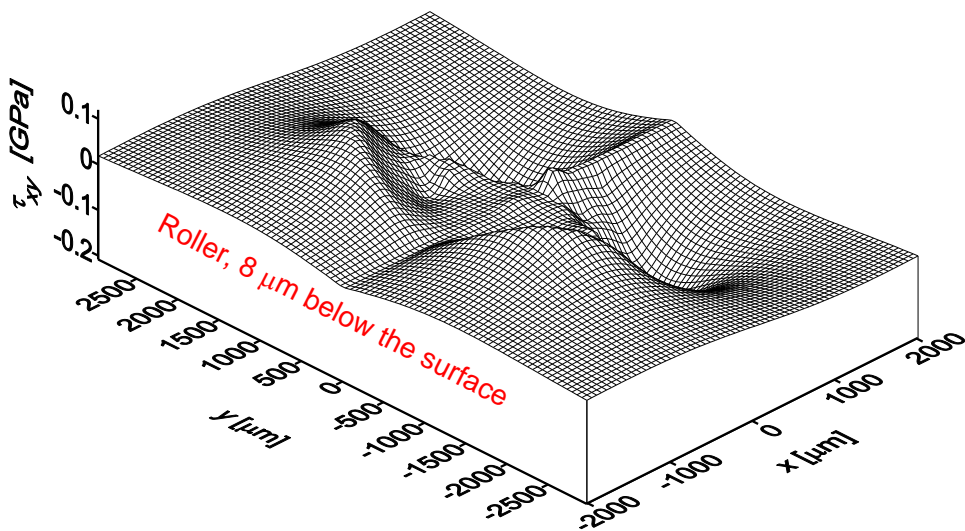


Figure 7.14 Distribution of shear stress τ_{xy} at $z = 8 \mu\text{m}$.

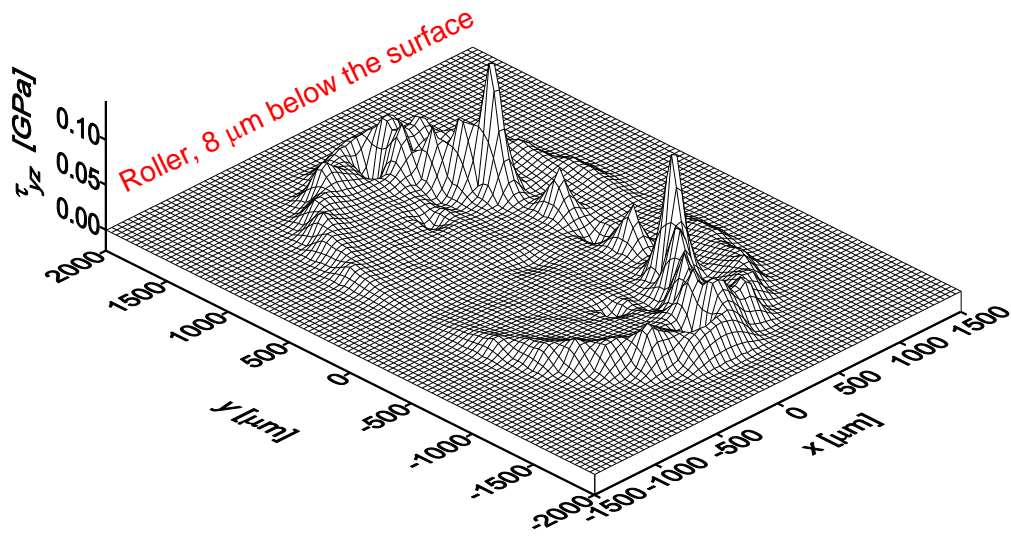


Figure 7.15 Distribution of shear stress τ_{yz} at $z = 8 \mu\text{m}$.

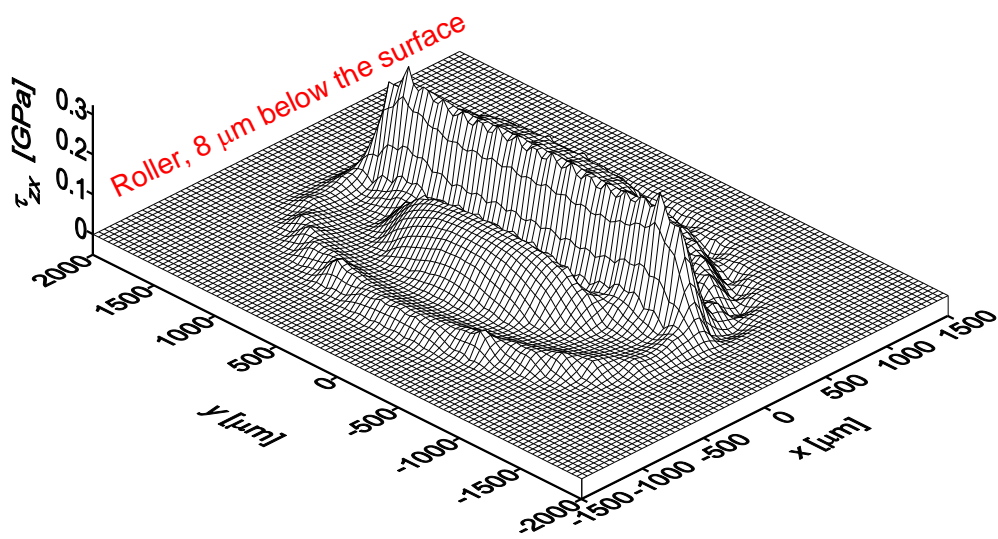


Figure 7.16 Distribution of shear stress τ_{zx} at $z = 8 \mu\text{m}$.

8. Discussion and suggestions

This section summarises the work done and gives suggestions to build an efficient test rig for experimenting on the operation of the main IVT variator components, namely the roller and the toroidal disk. It also provides hints on future work needed to complete the theoretical analysis and improve the present model.

The theoretical work carried out during this 18-month project covered the lubrication, loading and life expectancy aspects of the rollers and toroidal disks of a TOROTRAK IVT variator. The lubrication problem was modelled by means of a generalised Reynolds equation (§ 3.1) for transient, non-Newtonian analysis of rough, elliptical contacts, excluding lubricant thermal effects. The problem was attacked from a general point of view, including roughness asperity interactions (solid contact) in the analysis (but excluding a possible thermal displacement of rubbing asperities) in combination with the normal full-film-separation analysis. This way, the pressure and traction in the contact are calculated. Through this, the surface loading of the contact is established, which is then used to calculate the subsurface stress fields through a 3-dimensional analysis (§ 4). Finally, the subsurface stress results are used to calculate the life expectancy of the rollers and disks, based on the Ioannides-Harris fatigue life model (§ 5), with a choice of two suitable fatigue criteria (§ 5.1, 5.2).

Based on the examples analysed in § 7, it is seen that various factors can affect the operation of the examined contact. These factors are listed next.

- The lubricant operating temperature. It is shown and discussed in § 7 that the lubricant operating temperature plays an important role in the effective lubrication of the contact. According to TOROTRAK, the lubricant operating temperature is normally quite high, often 80 – 120 °C. Bulk temperatures over 100 °C are excessive, because they are associated with film thinning or collapse, depending on the roughness texture of the cooperating surfaces. It must be realised that these temperatures must be added to the local lubricant or solid temperatures in the contact, arising from frictional heating of the lubricant and/or roughness asperities. Lubricant frictional heating can give flash temperatures of around 50 - 100 °C, and asperity frictional heating (which is much more localised) can result in flash temperatures of 1000 °C or more! Moreover, lower lubricant operating temperature satisfies the traction demands of the contact obviously better than higher temperature (see also table 7.2).

Therefore, it is suggested that a proper cooling system be used that will feed the variator with sufficiently cool oil. The level of cooling can be determined by using the computer program of this project and calculate the film thickness and traction forces of particular cases; there are obviously other factors that must be accounted for (for example cost, feasibility, increased weight, design complications etc). In general, a lubricant operating temperature of around 80 °C (or lower) is much more preferable than temperatures in excess of 100 °C.

- The “severity” of surface roughness (RMS). As was shown in tables 7.2 and 7.3, the surface roughness texture and RMS value are very important in avoiding solid contact (asperity collisions), which result in localised thermoelastoplastic loading of the contact and, generally, reduce the fatigue life. This conclusion has also been presented in the literature (see for example Ai, 1998). In general, higher RMS values (overly rougher surfaces or surfaces with large bumps or roughness asperities) are associated with increased asperity interaction and, thus, solid contact.

It is, therefore, suggested that the working-surface finish of the main variator components (rollers and disks) be of a high standard, with RMS values of 0.2 or lower.

- Transient effects. Transient effects have been incorporated in the model and the accompanying computer program. It is known that, in a TOROTRAK variator, sudden changes of the transmitted load, the entraining speeds as well as changes of the working angle (angle φ in figure 7.3) *do* occur during the normal operation of the IVT. Such changes are transient phenomena and it is known that they can result in film thinning or collapse. Moreover, it is assumed in the model that there are no structural vibrations and, hence, the supported load is always equal to the transmitted load (see equation (3.58)). If there are structural vibrations (caused, for example, by engine vibrations or irregular road surfaces on which an IVT-equipped vehicle is driven), then the supported load is not equal to the load that has to be transmitted and their difference is equal to the difference in the inertial forces of the roller and the disk (i.e. there is a Newtonian acceleration term in the force equilibrium equation). This often means loss of film support that can be detected as noise (a similar phenomenon occurs during the dynamic loading of spur gears).

It is, therefore, suggested that the variator be isolated from the rest of the vehicle or working environment with shock absorbing materials and that the rotating parts of the variator be adequately balanced to minimise oscillations. It is also suggested that the changes of the working angle of the variator be electronically controlled to avoid excessive accelerations, and to follow a maximum predetermined rate of acceleration (rate of change of the working angle). The latter could be determined by using the present model and program to simulate a working scenario and study the transient film thickness as a function of the rate of change of the working angle (this is straightforward to do with the program because the working angle and the corresponding time are direct inputs to the program).

- The traction fluid limiting shear strength. For increased traction it is obviously important to use a traction fluid that has a high limiting shear strength (see also § 3.3). Using the present model and computer program, it was confirmed that, normally, a significant portion of the roller-disk contact operates under the lubricant's limiting shear stress. Traction results are thus very much dependent on the shear strength of the traction fluid.

The efficient design of a variator test rig must be based on the previous observations. More specifically:

1. The rig must use real working components, namely rollers and disks from the current production line. The roughness of the components must be representative of the roughness (texture and RMS magnitude) normally encountered in the end product.
2. The rig must have allowance to simulate a realistic operation scenario, i.e. a sequence of working angles, loads, and rotational speeds changes, that is considered representative of normal operation of the IVT. Predetermined speeds and loads that remain constant in time (i.e. a static rig), cannot yield reliable results and the fatigue lives may be overestimated.
3. The rig must include a device to control the lubricant operating temperature. The effects of altering that temperature can then be studied.
4. Although not of the highest priority (and definitely complex and expensive), it would be possible to measure vibrations of a foreign origin on the variator during normal operation (for example, when fitted on a moving vehicle) and then recreate

this external dynamic loading on the test rig. It could then be possible to see the effect of external vibrations on the effectiveness of lubrication and the fatigue lives of the main components, compared with the same values when operating in a vibration-free environment.

9. Computer program (“TORO.EXE”, version 1.0.0 beta)

One of the main targets of this project was the creation of a computer program to apply the developed model and use for quantified predictions. Such a program has indeed been created and some results can be seen in § 7. The code is written using the very latest FORTRAN language ANSI standard (FORTRAN 95) and compiled with the Lahey FORTRAN 95 compiler, version 5.5g with full optimisation. The input and output of the program involve several files, all of which are listed below.

It is noted that these files and their specific format are for version “1.0.0 beta” of the program. Future versions may use different formats.

Input file: tPfv.DAT		
<ul style="list-style-type: none"> This file must exist for the program to run. 		
Column	Variable	Unit
1	Time, t	s
2	Supported load, P	N
3	Working angle, φ (see figure 7.3)	deg (°)
4	Entraining speed of the roller in x, u_{roller}	m/s
5	Entraining speed of the toroidal disk in x, u_{disk}	m/s
6	Entraining speed of the roller in y, v_{roller}	m/s
7	Entraining speed of the toroidal disk in y, v_{disk}	m/s

Input file: xyROUGH1.DAT (optional)		
<ul style="list-style-type: none"> This optional file must contain the roughness data for the roller. The <u>first line</u> of this file must have the spatial steps of the roughness data, namely Δx and Δy (both in meters). 		
Column	Variable	Unit
1	x ($x \geq 0$, distance from an arbitrary reference point)	m
2	y ($-y_{\text{max}} \leq y \leq y_{\text{max}}$, i.e. symmetrical around zero)	m
3	Roughness of the roller, $\zeta_{\text{roller}}(x, y)$	μm

Input file: xyROUGH2.DAT (optional)		
<ul style="list-style-type: none"> • This optional file must contain the roughness data for the toroidal disk. • The <u>first line</u> of this file must have the spatial steps of the roughness data, namely Δx and Δy (both in meters). 		
Column	Variable	Unit
1	x ($x \geq 0$, distance from an arbitrary reference point)	m
2	y ($-y_{\max} \leq y \leq y_{\max}$, i.e. symmetrical around zero)	m
3	Roughness of the toroidal disk, $\zeta_{\text{disk}}(x, y)$	μm

Output file: TOROph.DAT		
<ul style="list-style-type: none"> • This file contains important results about the pressure, film thickness and the local traction coefficients. 		
Column	Variable	Unit
1	Time, t	s
2	x (x -distance from the centre of the contact)	μm
3	y (y -distance from the centre of the contact)	μm
4	Pressure, $p(x, y, t)$	Pa
5	Film thickness, $h(x, y, t)$	μm
6	Hertzian pressure at (x, y, t)	Pa
7	Local traction coefficient for the roller, $\mu_{\text{roller}}(x, y, t)$	
8	Local traction coefficient for the toroidal disk, $\mu_{\text{disk}}(x, y, t)$	

Output file: TOROtxy1.DAT		
<ul style="list-style-type: none"> This file contains traction results for the roller. 		
Column	Variable	Unit
1	Time, t	s
2	x (x-distance from the centre of the contact)	μm
3	y (y-distance from the centre of the contact)	μm
4	Traction on the roller in x, $\bar{\tau}_{zx}^{(\text{roller})}(x, y, t)$	Pa
5	Traction on the roller in y, $\bar{\tau}_{zy}^{(\text{roller})}(x, y, t)$	Pa
6	Resultant traction on the roller, $\sqrt{[\bar{\tau}_{zx}^{(\text{roller})}]^2 + [\bar{\tau}_{zy}^{(\text{roller})}]^2}$	Pa
7	Traction on the roller in x, over the local limiting shear stress, $\frac{\bar{\tau}_{zx}^{(\text{roller})}(x, y, t)}{\tau_L(x, y, t)}$	
8	Traction on the roller in y, over the local limiting shear stress, $\frac{\bar{\tau}_{zy}^{(\text{roller})}(x, y, t)}{\tau_L(x, y, t)}$	
9	Resultant traction on the roller, over the local limiting shear stress, $\frac{\sqrt{[\bar{\tau}_{zx}^{(\text{roller})}]^2 + [\bar{\tau}_{zy}^{(\text{roller})}]^2}}{\tau_L(x, y, t)}$	

Output file: TOROtxy2.DAT		
<ul style="list-style-type: none"> This file contains traction results for the toroidal disk. 		
Column	Variable	Unit
1	Time, t	s
2	x (x-distance from the centre of the contact)	μm
3	y (y-distance from the centre of the contact)	μm
4	Traction on the toroidal disk in x, $\bar{\tau}_{zx}^{(\text{disk})}(x, y, t)$	Pa
5	Traction on the toroidal disk in y, $\bar{\tau}_{zy}^{(\text{disk})}(x, y, t)$	Pa
6	Resultant traction on the toroidal disk, $\sqrt{[\bar{\tau}_{zx}^{(\text{disk})}]^2 + [\bar{\tau}_{zy}^{(\text{disk})}]^2}$	Pa
7	Traction on the toroidal disk in x, over the local limiting shear stress, $\frac{\bar{\tau}_{zx}^{(\text{disk})}(x, y, t)}{\tau_L(x, y, t)}$	
8	Traction on the toroidal disk in y, over the local limiting shear stress, $\frac{\bar{\tau}_{zy}^{(\text{disk})}(x, y, t)}{\tau_L(x, y, t)}$	
9	Resultant traction on the toroidal disk, over the local limiting shear stress, $\frac{\sqrt{[\bar{\tau}_{zx}^{(\text{disk})}]^2 + [\bar{\tau}_{zy}^{(\text{disk})}]^2}}{\tau_L(x, y, t)}$	

Output file: tPfvab.DAT		
<ul style="list-style-type: none"> This file contains the dimensions of the contact ellipse. The results may be interpolated through time steps. 		
Column	Variable	Unit
1	Time, t	s
2	Supported load, P	N
3	Working angle, φ (see figure 7.3)	deg (°)
4	Entraining speed of the roller in x, u_{roller}	m/s
5	Entraining speed of the toroidal disk in x, u_{disk}	m/s
6	Entraining speed of the roller in y, v_{roller}	m/s
7	Entraining speed of the toroidal disk in y, v_{disk}	m/s
8	Length of the contact-ellipse semi-axis x, D_x	μm
9	Length of the contact-ellipse semi-axis y, D_y	μm

Output file: thp.DAT		
<ul style="list-style-type: none"> This file contains results about the film thickness and the overall traction coefficients. 		
Column	Variable	Unit
1	Time, t	s
2	Central film thickness, $h(0,0,t)$	μm
3	Minimum film thickness, $h_{\text{min}}(t)$	μm
4	Maximum Hertzian pressure, $p_0(t)$	GPa
5	Overall traction coefficient for the roller, $\mu_{\text{roller}}(t)$	
6	Overall traction coefficient for the toroidal disk, $\mu_{\text{disk}}(t)$	

Output file: txyzs1t1.DAT (optional)		
<ul style="list-style-type: none"> This optional file contains subsurface-stress results for the roller. 		
Column	Variable	Unit
1	Time, t	s
2	x (x-distance from the centre of the contact)	μm
3	y (y-distance from the centre of the contact)	μm
4	z (z-distance from the surface, below the surface)	μm
5	$\sigma_{xx}^{(\text{roller})}(x, y, z, t)$	Pa
6	$\sigma_{yy}^{(\text{roller})}(x, y, z, t)$	Pa
7	$\sigma_{zz}^{(\text{roller})}(x, y, z, t)$	Pa
8	$\tau_{xy}^{(\text{roller})}(x, y, z, t)$	Pa
9	$\tau_{yz}^{(\text{roller})}(x, y, z, t)$	Pa
10	$\tau_{zx}^{(\text{roller})}(x, y, z, t)$	Pa

Output file: txyzs2t2.DAT (optional)		
<ul style="list-style-type: none"> This optional file contains subsurface-stress results for the toroidal disk. 		
Column	Variable	Unit
1	Time, t	s
2	x (x-distance from the centre of the contact)	μm
3	y (y-distance from the centre of the contact)	μm
4	z (z-distance from the surface, below the surface)	μm
5	$\sigma_{xx}^{(\text{disk})}(x, y, z, t)$	Pa
6	$\sigma_{yy}^{(\text{disk})}(x, y, z, t)$	Pa
7	$\sigma_{zz}^{(\text{disk})}(x, y, z, t)$	Pa
8	$\tau_{xy}^{(\text{disk})}(x, y, z, t)$	Pa
9	$\tau_{yz}^{(\text{disk})}(x, y, z, t)$	Pa
10	$\tau_{zx}^{(\text{disk})}(x, y, z, t)$	Pa

REFERENCES

Ai, X., 1998, "Effect of Three-Dimensional Random Surface Roughness on Fatigue Life of a Lubricated Contact", *ASME Journal of Tribology*, Vol. 120, pp. 159-164.

Ai, X., Cheng, H. S., and Zheng, L., 1993, "A Transient Model for Micro-Elastohydrodynamic Lubrication With Three-Dimensional Irregularities", *ASME Journal of Tribology*, Vol. 115, pp. 102-110.

Ai, X., and Linqing, Z., 1989, "A General Model for Microelastohydrodynamic Lubrication and Its Full Numerical Solution", *ASME Journal of Tribology*, Vol. 111, pp. 569-576.

Ai, X., and Yu, H., 1988, "A Full Numerical Solution for General Transient Elastohydrodynamic Line Contacts and Its Application", *WEAR*, Vol. 121, pp. 143-159.

Archard, J. F., 1973, "Elastohydrodynamic Lubrication of Real Surfaces", *TRIBOLOGY*, February 1973, pp. 8-14.

Bailey, D. M., and Sayles, R. S., 1991, "Effect of Roughness and Sliding Friction on Contact Stresses", *ASME Journal of Tribology*, Vol. 113, pp. 729-737.

Bair, S., and Winer, W. O., 1979, "A Rheological Model for Elastohydrodynamic Contacts Based in Primary Laboratory Data", *ASME Journal of Lubrication Technology*, Vol. 101, No. 3, pp. 258-265.

Bartz, W. J., and Krüger, V., 1973, "Pitting Fatigue of Gears – Some Ideas on Appearance, Mechanism and Lubricant Influence", *TRIBOLOGY*, October 1973, pp. 191-195.

- Berthe, D., and Godet, M.,** 1974, “Elastohydrodynamic Lubrication of Rough Surfaces in Pure Rolling”, *TRIBOLOGY INTERNATIONAL*, April 1974, pp. 67-69.
- Biao, L. S., Ju, M. J., and Yang, C. X.,** 1993, “Elliptic-Paraboloid Method for Calculating Surface Elastic Deformation in EHL”, *TRIBOLOGY INTERNATIONAL*, Vol. 26, No. 6, pp. 443-448.
- Bissett, E. J., and Glander, D. W.,** 1988, “A Highly Accurate Approach That Resolves the Pressure Spike of Elastohydrodynamic Lubrication”, *ASME Journal of Tribology*, Vol. 110, pp. 241-246.
- Biswas, S., and Snidle, R. W.,** 1977, “Calculation of Surface Deformation in Point Contact EHD”, *ASME Journal of Lubrication Technology*, Vol. 99, pp. 313-317.
- Cameron, A.,** 1966, *The Principles of Lubrication*, Longmans, London.
- Chang, L.,** 1992, “Traction in Thermal Elastohydrodynamic Lubrication of Rough Surfaces”, *ASME Journal of Tribology*, Vol. 114, pp. 186-191.
- Chang, L.,** 1995, “Deterministic Modeling and Numerical Simulation of Lubrication Between Rough Surfaces – a Review of Recent Developments”, *WEAR*, Vol. 184, pp. 155-160.
- Chang, L., Cusano, C., and Conry, T. F.,** 1989, “Effects of Lubricant Rheology and Kinematic Conditions on Micro-Elastohydrodynamic Lubrication”, *ASME Journal of Tribology*, Vol. 111, pp. 344-351.
- Chang, L., and Gao, Y.,** 1999, “A Simple Numerical Method for Contact Analysis of Rough Surfaces”, *ASME Journal of Tribology*, Vol. 121, pp. 425-432.
- Chang, L., and Webster, M. N.,** 1991, “A Study of Elastohydrodynamic Lubrication of Rough Surfaces”, *ASME Journal of Tribology*, Vol. 113, pp. 110-115.

Chou, C. C., and Lin, J. F., 1997, "Tribological Effects of Roughness and Running-In on Oil-Lubricated Line Contacts", *IMEchE Journal of Engineering Tribology*, Vol. 211, pp. 209-222.

Demuren, A. O., 1989, "Application of Multi-Grid Methods for Solving the Navier-Stokes Equations", *IMEchE Journal of Mechanical Engineering Science*, Vol. 203, pp. 255-265.

Dowson, D., and Higginson, G. R., 1966, *Elasto-hydrodynamic Lubrication, The Fundamentals of Roller and Gear Lubrication*, Pergamon Press, Oxford.

Dwyer-Joyce, R. S., 1993, "The Effects of Lubricant Contamination on Rolling Bearing Performance", Ph.D. thesis, Imperial College of Science, Technology and Medicine, Mechanical Engineering Department, Tribology Section, London, England.

Ehret, P., Dowson, D., and Taylor, C. M., 1999, "Transient EHL Solutions With Interfacial Slip", *ASME Journal of Tribology*, Vol. 121, pp. 703-710.

Elcoate, C. D., 1996, "Coupled Solution Methods for the Elastohydrodynamic Lubrication Problem", Ph.D. thesis, Division of Mechanical Engineering, School of Engineering, University of Wales, Cardiff.

Elsharkawy, A. A., and Hamrock, B. J., 1991, "Subsurface Stresses in Micro-EHL Line Contacts", *ASME Journal of Tribology*, Vol. 113, No. 3, pp. 645-656.

Evans, C. R., and Johnson, K. L., 1987, "The Influence of Surface Roughness on Elastohydrodynamic Traction", *Proceedings of the IMechE*, Vol. 201, pp. 145-151.

Evans, H. P., and Snidle, R. W., 1981, "Inverse Solution of Reynolds' Equation of Lubrication Under Point-Contact Elastohydrodynamic Conditions", *ASME Journal of Lubrication Technology*, Vol. 103, pp. 539-546.

Fang, N., Chang, L., and Johnston, G. J., 1999, "Some Insights into Micro-EHL Pressures", *ASME Journal of Tribology*, Vol. 121, pp. 473-480.

Fenner, R. T., 1986, *Engineering Elasticity*, Wiley.

Gahouet, V., Baillet, L., Meurisse, M. H., and Bou-Saïd, B., 1999, "Direct and Indirect Approaches at the Plasto-Hydrodynamic Lubrication Problem. Application to an Industrial Ironing Process", *ASME Journal of Tribology*, Vol. 121, pp. 523-528.

Gecim, B., and Winer, W. O., 1980, "Lubricant Limiting Shear Stress Effect on EHD Film Thickness", *ASME Journal of Lubrication Technology*, Vol. 102, p. 213.

Glander, D. W., and Bissett, E. J., 1988, "On the Stability and Uniqueness of Elastohydrodynamic Lubrication Solutions", *ASME Journal of Tribology*, Vol. 110, pp. 628-631.

Greenwood, J. A., and Morales-Espejel, G. E., 1994, "The Behaviour of Transverse Roughness in EHL Contacts", *IMechE Journal of Engineering Tribology*, Vol. 208, pp. 121-132.

Greenwood, J. A., and Tripp, J. H., 1971, "The Contact of Two Nominally Flat Rough Surfaces", *Proceedings of the IMechE (1970-71)*, Vol. 185, pp. 625-633.

Hamer, J. C., Sayles, R. S., and Ioannides, E., 1990, "The Collapse of Sliding Micro-EHL Films by Plastic Extrusion", *ASME Journal of Tribology*, paper No. 90-Trib-47.

Hamrock, B. J., 1994, *Fundamentals of Fluid Film Lubrication*, McGraw-Hill.

Hamrock, B. J., and Brewe, D. E., 1983, "Simplified Solution for Stresses and Deformations", *ASME Journal of Lubrication Technology*, Vol. 105, No. 2, pp. 171-177.

Hamrock, B. J., Pan, P., and Lee, R.-T., 1988, "Pressure Spikes in Elastohydrodynamically Lubricated Conjunctions", *ASME Journal of Tribology*, Vol. 110, pp. 279-284.

Harris, T., Ioannides, E., Ragen, M., and Tam, H., 1990, “Endurance of Aircraft Gas Turbine Mainshaft Ball Bearings – Analysis Using Improved Fatigue Life Theory: Part 2 – Application to a Bearing Operating Under Difficult Lubrication Conditions”, *ASME Journal of Tribology*, Vol. 112, pp. 309-316.

Hooke, C. J., 1994, “The Minimum Film Thickness in Lubricated Line Contacts During a Reversal of Entrainment – General Solution and the Development of a Design Chart”, *IMEchE Journal of Engineering Tribology*, Vol. 208, pp. 53-64.

Hooke, C. J., 1998, “Surface Roughness Modification in Elastohydrodynamic Line Contacts Operating in the Elastic Piezoviscous Regime”, *IMEchE Journal of Engineering Tribology*, Vol. 212, pp. 145-162.

Hornig, J. H., 1998, “An Elliptic Elastic-Plastic Asperity Microcontact Model for Rough Surfaces”, *ASME Journal of Tribology*, Vol. 120, pp. 82-88.

Hou, K., Zhu, D., and Wen, S., 1985, “A New Numerical Technique for Computing Surface Elastic Deformation Caused by a Given Normal Pressure Distribution”, *ASME Journal of Tribology*, Vol. 107, pp. 128-131.

Houpert, L. G., and Hamrock, B. J., 1986, “Fast Approach for Calculating Film Thicknesses and Pressures in Elastohydrodynamically Lubricated Contacts at High Loads”, *ASME Journal of Tribology*, Vol. 108, pp. 411-420.

Ioannides, E., and Harris, T. A., 1985, “A New Fatigue Life Model for Rolling Bearings”, *ASME Journal of Tribology*, Vol. 107, pp. 367-378.

Ioannides, E., Harris, T. A., and Ragen, M., 1990, “Endurance of Aircraft Gas Turbine Mainshaft Ball Bearings – Analysis Using Improved Fatigue Life Theory: Part 1 – Application to a Long-Life Bearing”, *ASME Journal of Tribology*, Vol. 112, pp. 304-308.

Jacobson, B., Ioannides, E., and Tripp, J. H., 1988, “Redistribution of Solidified Films in Rough Hertzian Contacts. Part I: Theory”, *Proceedings of the 14th Leeds-*

Lyon Symposium on Tribology, 8-11 September 1987, Elsevier, Tribology series, 12, pp. 51-57.

Jiang X., Hua, D. Y., Cheng, H. S., Ai, X., and Lee, S. C., “A Mixed Elastohydrodynamic Lubrication Model With Asperity Contact”, *ASME Journal of Tribology*, Vol. 121, pp. 481-491.

Johnson, K. L., 1985, *Contact Mechanics*, (reprint 1994), Cambridge University Press.

Kannel, J. W., and Tevaarwerk, J. L., 1984, “Subsurface Stress Evaluations Under Rolling/Sliding Contacts”, *ASME Journal of Tribology*, Vol. 106, pp. 96-103.

Kennedy, F. E. Jr., 1984, “Thermal and Thermomechanical Effects in Dry Sliding”, *WEAR*, Vol. 100, pp. 453-476.

Khonsari, M. M., and Hua, D. Y., 1993, “Generalized Non-Newtonian Elastohydrodynamic Lubrication”, *TRIBOLOGY INTERNATIONAL*, Vol. 26, No. 6, pp. 405-411.

Kim, K. H., and Sadeghi, F., 1992, “Three-Dimensional Temperature Distribution in EHD Lubrication: Part I – Circular Contact”, *ASME Journal of Tribology*, Vol. 114, pp. 32-41.

Kweh, C. C., Evans, H. P., and Snidle, R. W., 1989, “Elastohydrodynamic Lubrication of Heavily Loaded Circular Contacts”, *IMechE Journal of Mechanical Engineering Science*, Vol. 203, pp. 133-148.

Kweh, C. C., Evans, H. P., and Snidle, R. W., 1989, “Micro-Elastohydrodynamic Lubrication of an Elliptical Contact With Transverse and Three-Dimensional Sinusoidal Roughness”, *ASME Journal of Tribology*, Vol. 111, pp. 577-584.

Lee, R. T., and Hamrock, B. J., 1990a, “A Circular Non-Newtonian Fluid Model: Part I – Used in Elastohydrodynamic Lubrication”, *ASME Journal of Tribology*, Vol. 112, No. 3, pp. 486-496.

Lee, R. T., and Hamrock, B. J., 1990b, “A Circular Non-Newtonian Fluid Model: Part II – Used in Microelastohydrodynamic Lubrication”, *ASME Journal of Tribology*, Vol. 112, No. 3, pp. 497-505.

Lee-Prudhoe, I., Sayles, R. S., and Kaderic, A., 1999, “Investigations Into Asperity Persistence in Heavily Loaded Contacts”, *ASME Journal of Tribology*, Vol. 121, pp. 441-448.

Lin, J.-F., and Chu, H. Y., 1991, “A Numerical Solution for Calculating Elastic Deformation in Elliptical-Contact EHL of Rough Surface”, *ASME Journal of Tribology*, Vol. 113, pp. 12-21.

Lin, J.-F., and Horng, J. H., 1992, “Analyses of Thermal Hydrodynamic Lubrication in High-Speed Rolling. Part II: the Effect of Non-Newtonian Viscosity Models”, *TRIBOLOGY INTERNATIONAL*, Vol. 25, No. 5, pp. 341-349.

Lin, T.-R., and Lin, J.-F., 1991, “Thermal Effects in Elastohydrodynamic Lubrication of Line Contacts Using a Non-Newtonian Lubricant”, *TRIBOLOGY INTERNATIONAL*, Vol. 24, No. 6, pp. 365-372.

Lu, C.-J., and Bogy, D. B., 1992, “The Influence of Thermal Deformation on the Contact Temperature of Sliding Asperities”, *ASME Journal of Applied Mechanics*, Vol. 59, pp. 102-106.

Lubrecht, A. A., Dwyer-Joyce, R. S., and Ioannides, E., 1992, “Analysis of the Influence of Indentations on Contact Life”, *Proceedings of the 18th Leeds-Lyon Symposium on Tribology*, 3-6 September 1991, Elsevier, Tribology Series, 21, pp. 173-181.

Lubrecht, A. A., Jacobson, B. O., and Ioannides, E., 1990, "Lundberg Palmgren Revisited", Rolling Element Bearings – towards the 21st Century, Seminar organised by IMechE (16 November 1990), pp. 17-20.

Lubrecht, A. A., ten Napel, W. E., and Bosma, R., 1986, "Multigrid, an Alternative Method for Calculating Film Thickness and Pressure Profiles in Elastohydrodynamically Lubricated Line Contacts", *ASME Journal of Tribology*, Vol. 108, pp. 551-556.

Mokhtar, M. O. A., and Ghany, A. A. A., 1985, "Elastohydrodynamic Behavior of Rolling Elliptical Contacts: Part I: Pressure and Temperature Distributions", *ASME Journal of Tribology*, Vol. 107, pp. 343-351.

Mokhtar, M. O. A., and Ghany, A. A. A., 1985, "Elastohydrodynamic Behavior of Rolling Elliptical Contacts: Part II: Oil Film Thickness and Contact Profile", *ASME Journal of Tribology*, Vol. 107, pp. 352-358.

Moore, A. J., 1997, "The Behaviour of Lubricants in Elastohydrodynamic Contacts", *IMechE Journal of Engineering Tribology*, Vol. 211, pp. 91-106.

Mostofi, A., and Gohar, R., 1983, "Elastohydrodynamic Lubrication of Finite Line Contacts", *ASME Journal of Lubrication Technology*, Vol. 105, pp. 598-604.

Nikas, G. K., 1999, "Theoretical Modelling of the Entrainment and Thermomechanical Effects of Contamination Particles in Elastohydrodynamic Contacts", Ph.D. thesis, Imperial College of Science, Technology and Medicine, Mechanical Engineering Department, Tribology Section, London.

Nikas, G. K., Sayles, R. S., and Ioannides, E., 1999, "Thermoelastic Distortion of EHD Line Contacts During the Passage of Soft Debris Particles", *ASME Journal of Tribology*, Vol. 121, No 2, pp. 265-271.

- Osborn, K. F., and Sadeghi, F.,** 1992, "Time Dependent Line EHD Lubrication Using the Multigrid/Multilevel Technique", *ASME Journal of Tribology*, Vol. 114, pp. 68-74.
- Patir, N., and Cheng, H. S.,** 1978, "An Average Flow Model for Determining Effects of Three-Dimensional Roughness on Partial Hydrodynamic Lubrication", *ASME Journal of Lubrication Technology*, Vol. 100, pp. 12-17.
- Patterson, M.,** 1991, "Traction Drive Contact Optimisation", *Proceedings of the 17th Leeds-Lyon Symposium on Tribology*, 4-7 September 1990, Elsevier, Tribology series, 18, pp. 295-300.
- Press, W. H., Teukolsky, S. A., Vetterling, W. T., and Flannery, B. P.,** 1992, *Numerical Recipes in FORTRAN*, second edition, Cambridge University Press.
- Prakash, J., and Czichos, H.,** 1983, "Influence of Surface Roughness and Its Orientation on Partial Elastohydrodynamic Lubrication of Rollers", *ASME Journal of Lubrication Technology*, Vol. 105, pp. 591-596.
- Rhatigan, J. L., Johnson, R. R., and Dow, T. A.,** 1989, "An Experimental Study of Thermoelastic Effects in Scuffing Failure of Sliding Lubricated Contacts", *ASME Journal of Tribology*, Vol. 111, pp. 23-28.
- Roelands, C. J. A.,** 1966, "Correlation Aspects of the Viscosity-Temperature-Pressure Relationship of Lubricating Oils", Ph.D. thesis, Technische Hogeschool, Delft, The Netherlands.
- Roelands, C. J. A., Vlugter, J. C., and Waterman, H. I.,** 1963, "The Viscosity-Temperature-Pressure Relationship of Lubricating Oils and Its Correlation With Chemical Constitution", *ASME Journal of Basic Engineering*, Vol. 85, pp. 601-607.
- Rohde, S. M., Whicker, D., and Booker, J. F.,** 1979, "Elastohydrodynamic Squeeze Films: Effects of Viscoelasticity and Fluctuating Load", *ASME Journal of Lubrication Technology*, Vol. 101, pp. 74-80.

Rohde, S. M., Whicker, D., and Browne, A. L., 1976, "Dynamic Analysis of Elastohydrodynamic Squeeze Films", *ASME Journal of Lubrication Technology*, Vol. 98, pp. 401-408.

Sadeghi, F., and Sui, P. C., 1990, "Thermal Elastohydrodynamic Lubrication of Rough Surfaces", *ASME Journal of Tribology*, Vol. 112, pp. 341-346.

Sayles, R. S., 1996, "Basic Principles of Rough Surface Contact Analysis Using Numerical Methods", *TRIBOLOGY INTERNATIONAL*, Vol. 29, pp. 639-650.

Sayles, R. S., 1997, "A Contact-Fatigue Model for CVTs", Research Proposal for TOROTRAK DEVELOPMENT LTD, Imperial College, Mechanical Engineering Department, Tribology section, London, SW7 2BX.

Shieh, J.-A., and Hamrock, B. J., 1991, "Film Collapse in EHL and Micro-EHL", *ASME Journal of Tribology*, Vol. 113, pp. 372-377.

Stachowiak, G. W., and Batchelor, A. W., 1993, *Engineering Tribology*, Elsevier, Tribology Series, 24.

Stolarski, T. A., 1989, "Probability of Scuffing in Lubricated Contacts", *IMEchE Journal of Mechanical Engineering Science*, Vol. 203, pp. 361-369

Sui, P. C., and Sadeghi, F., 1991, "Thermoelastic Effects in Lubricated Rolling/Sliding Line Contacts", *ASME Journal of Tribology*, Vol. 113, pp. 174-181.

Sutcliffe, M. P. F., 1989, "Central Film Thicknesses in Elliptical Contacts", *IMEchE Journal of Mechanical Engineering Science*, Vol. 203, pp. 387-392.

Tieu, A. K., and Worden, J., 1987, "Transient Oil Film Thickness in Gear Contacts Under Dynamic Loads", *Proceedings of the 13th Leeds-Lyon Symposium on Tribology*, 8-12 September 1986, Elsevier, Tribology series, 11, pp. 285-290.

Ting, B.-Y., and Winer, W. O., 1989, "Friction Induced Thermal Influences in Elastic Contact Between Spherical Asperities", *ASME Journal of Tribology*, Vol. 111, pp. 315-322.

Tripp, J. H., 1983, "Surface Roughness Effects in Hydrodynamic Lubrication: The Flow Factor Method", *ASME Journal of Lubrication Technology*, Vol. 105, pp. 458-465.

Venner, C. H., 1991, "Multilevel Solution of the EHL Line and Point Contact Problems", Ph.D. thesis, University of Twente, The Netherlands.

Venner, C. H., and Lubrecht, A. A., 1994, "Transient Analysis of Surface Features in an EHL Line Contact in the Case of Sliding", *ASME Journal of Tribology*, Vol. 116, pp. 186-193.

Venner, C. H., ten Napel, W. E., and Bosma, R., 1990, "Advanced Multilevel Solution of the EHL Line Contact Problem", *ASME Journal of Tribology*, Vol. 112, pp. 426-432.

Vichard J. P., 1971, "Transient Effects in the Lubrication of Hertzian Contacts", *Journal of Mechanical Engineering Science*, Vol. 13, No. 3, pp. 173-189.

Wang, J. M., and Aronov, V., 1997, "Thermal Elastohydrodynamic Lubrication of Non-Newtonian Fluids With Rough Surfaces", *ASME Journal of Tribology*, Vol. 119, pp. 605-612.

Wang, S., Cusano, C., and Conry, T. F., 1991, "Thermal Analysis of Elastohydrodynamic Lubrication of Line Contacts Using the Ree-Eyring Fluid Model", *ASME Journal of Tribology*, Vol. 113, pp. 232-244.

Webster, M. N., Ioannides, E., and Sayles, R. S., 1986, "The Effect of Topographical Defects on the Contact Stress and Fatigue Life in Rolling Element Bearings", Mechanisms and Surface Distress, *Proceedings of the 12th Leeds-Lyon Symposium on Tribology*, 3-6 September 1985, Butterworths, pp. 207-221.

Webster, M. N., and Sayles, R. S., 1986, "A Numerical Model for the Elastic Frictionless Contact of Real Rough Surfaces", *ASME Journal of Tribology*, Vol. 108, pp. 314-320.

West, M. A., and Sayles, R. S., 1988, "A 3-Dimensional Method of Studying 3-Body Contact Geometry and Stress on Real Rough Surfaces", *Proceedings of the 14th Leeds-Lyon Symposium on Tribology*, 8-11 September 1987, Elsevier, Tribology series, 12, pp. 195-200.

Wong, P. L., Wang, R., and Lingard, S., 1996, "Pressure and Temperature Dependence of the Density of Liquid Lubricants", *WEAR*, Vol. 201, pp. 58-63.

Wu, Y.-W., and Yan, S.-M., 1987, "A Full Numerical Solution for the Non-Steady State Elastohydrodynamic Problem in Nominal Line Contacts", *Proceedings of the 13th Leeds-Lyon Symposium on Tribology*, 8-12 September 1986, Elsevier, Tribology series, 11, pp. 291-298.

Xu, G., Sadeghi, F., and Cogdell, D. J., 1997, "Debris Denting Effects on Elastohydrodynamic Lubricated Contacts", *ASME Journal of Tribology*, Vol. 119, pp. 579-587.

Yang, P., and Wen, S., 1990a, "A Generalized Reynolds Equation for Non-Newtonian Thermal Elastohydrodynamic Lubrication", *ASME Journal of Tribology*, Vol. 112, pp. 631-636.

Yang, P., and Wen, S., 1990b, "A Forward Iterative Numerical Method for Steady-State Elastohydrodynamically Lubricated Line Contacts", *TRIBOLOGY INTERNATIONAL*, Vol. 23, No. 1, pp. 17-22.

Yang, P., and Wen, S., 1992, "The Behavior of Non-Newtonian Thermal EHL Film in Line Contacts at Dynamic Loads", *ASME Journal of Tribology*, Vol. 114, pp. 81-85.

-
- Yang, P., and Wen, S.,** 1993, “A Fast, Robust, Straightforward Algorithm for Thermal Elastohydrodynamic Lubrication”, *TRIBOLOGY INTERNATIONAL*, Vol. 26, No. 1, pp. 17-23.
- Zhu, D., and Ai, X.,** 1997, “Point Contact EHL Based on Optically Measured Three-Dimensional Rough Surfaces”, *ASME Journal of Tribology*, Vol. 119, pp. 375-384.
- Zhu, D., and Cheng, H. S.,** 1988, “Effect of Surface Roughness on the Point Contact EHL”, *ASME Journal of Tribology*, Vol. 110, pp. 32-37.
- Zhu, D., and Wen, S.-Z.,** 1984, “A Full Numerical Solution for the Thermoelastohydrodynamic Problem in Elliptical Contacts”, *ASME Journal of Tribology*, Vol. 106, pp. 246-254.
- Zou, Q., Huang, C., and Wen, S.,** 1999, “Elastohydrodynamic Film Thickness in Elliptical Contacts With Spinning and Rolling”, *ASME Journal of Tribology*, Vol. 121, pp. 686-692.